

Optimal Ratchet Potentials for Run-and-Tumble particles

Zigan Zhen^{1,2} and Gunnar Pruessner^{1,2}

¹*Department of Mathematics, 180 Queen's Gate,
Imperial College London, SW7 2AZ London*

²*Centre for Complexity Science, Imperial College London**

(Dated: April 11, 2022)

Run-and-Tumble particles, mimicking the behaviour of microorganisms like *E. coli*, are a paradigmatic model of active matter. Due to self-propulsion, their random and undirected motion can be rectified in a ratchet potential. Using perturbative field theory, we determine the shape of the potential that produces the maximum particle current as a function of the particles' parameters.

Active matter systems, operating away from equilibrium, are composed of agents that consume energy from the environment to exert mechanical work [1]. Even when their motion is isotropic in free space, they can break detailed-balance by producing a spontaneous and directional motion in asymmetric environments [2–11] such as moving a ratchet wheel [12]. Such directed motion is known to control activated events in glassy systems [13], transport biological molecules [14–21] and revert the Ostwald process in active fluids [22]. Compared to the many observational studies, relatively little theoretical progress has been made to quantify and optimise non-equilibrium transport from first principles [4, 10, 23].

In the present work, we find the periodic ratchet potential that optimises the steady-state current of one-dimensional Run-and-Tumble (RnT) particles [24]. These are diffusive particles that move ballistically by self-propulsion until they change direction instantaneously and spontaneously under a Poisson process [25], taking place symmetrically in both directions. Feynman famously used a ratchet to illustrate that useful work cannot be extracted from diffusive particles [26]. That the random motion of RnT particles can be rectified at all is somewhat counter-intuitive and possible only because the spatial scale of the external potential is commensurate with the particles' mean free path [2–4, 27].

Rectified unidirectional motion of RnT particles in an asymmetric sawtooth potential has been investigated both theoretically and experimentally in [4, 8, 11, 12]. The locomotion of *E. coli* can be rectified by means of microfluidic funnels, which were further studied through theoretical models and numerical simulations [16]. Such studies have illustrated the far-reaching technological implications of active

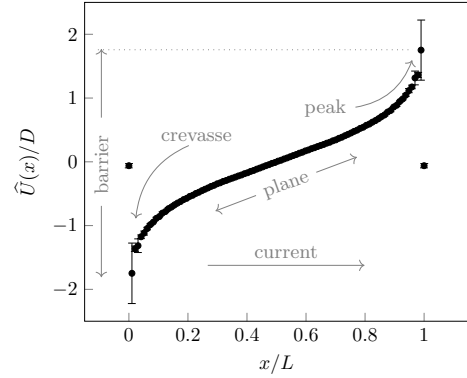


FIG. 1: Optimal potential $\widehat{U}(x)/D$ for $D = 1$, $w = 1$, $L = 1$ and $\gamma = 1$, so that $Pe = Qe = \kappa = 1$, resulting in the current $\widehat{J}L^2/D = 0.03789\dots$ to the right and $\widehat{\nu}_{\text{r0c}} = 1.167\dots$. The details of the numerical scheme employed to produce the plot are discussed in Suppl. A2.

particles for example for drug delivery or for separating particle species by activity. Despite the efforts made in experimental and numerical studies [20, 28], not a lot of light has been shed on the design principles of optimal transportation of active particles in ratchets. Extending well beyond existing work on RnT particles in specific potentials [4, 8], in the following we consider completely general potentials in a perturbative field theory, without making any approximations. While the perturbation theory can equally be implemented using classical methods, the field theory provides a systematic, diagrammatic framework to keep track of the contribution at every order. We subsequently use a numerical scheme to find the potential, such as Fig. 1, that maximises the particle current.

Model and method. In this work, we study a single RnT particle with position $x(t) \in [0, L]$ in a potential $\Phi(x)$ on a ring with circumference L . The motion is governed by the Langevin equation

$$\dot{x}(t) = -\Phi'(x) + wu(t) + \sqrt{2D}\xi(t), \quad (1)$$

* Correspondence email address:
g.pruessner@imperial.ac.uk

where $\Phi'(x)$ is the derivative of $\Phi(x)$, w is the particle's self-propulsion speed, $u(t)$ is a telegraphic noise switching between 1 and -1 with Poissonian rate γ and $\xi(t)$ is a unit Gaussian white noise with correlator $\langle \xi(t)\xi(t') \rangle = 2D\delta(t-t')$ and diffusion constant D . The motion Eq. (1) is subject to periodic boundary conditions with period L and $x \in [0, L)$, so that the process has a steady state and effectively $\Phi(x) = \Phi(x+L)$. Due to the self-propulsion, the system is driven out of equilibrium and its invariant measure is generically not of Boltzmann form $\rho(x) \propto e^{-\Phi(x)/D}$.

Field theory. In what follows, we calculate the steady-state density $\rho(x)$ of an RnT particle Eq. (1), as well as its steady-state current J in a perturbation theory in the coupling ν to the arbitrary potential $U(x)$, such that $\Phi(x) = \nu U(x)$. To this end, we cast the RnT dynamics in the language of a Doi-Peliti field theory [25, 29–33] as detailed in Suppl. B. Observables are more conveniently expressed in frequencies ω instead of direct time t and discretised modes $k_a = 2\pi a/L$ instead of real space, Eq. (B10).

The propagators can then be written in a perturbation theory about $\nu = 0$. Using the potential vertices Eq. (B18), each propagator picks up 2^n contributions to order n in the perturbation theory, for example

$$\begin{aligned} & \left\langle \phi_a(\omega) \tilde{\phi}_b(\omega') \right\rangle \\ & \triangleq \text{---} + \text{---} \overset{\text{---}}{\underset{\circ}{\text{---}}} + \text{---} \overset{\text{---}}{\underset{\circ}{\text{---}}} \text{---} \\ & + \text{---} \overset{\text{---}}{\underset{\circ}{\text{---}}} \overset{\text{---}}{\underset{\circ}{\text{---}}} + \text{---} \overset{\text{---}}{\underset{\circ}{\text{---}}} \overset{\text{---}}{\underset{\circ}{\text{---}}} \text{---} \\ & + \text{---} \overset{\text{---}}{\underset{\circ}{\text{---}}} \overset{\text{---}}{\underset{\circ}{\text{---}}} \text{---} + \text{---} \overset{\text{---}}{\underset{\circ}{\text{---}}} \overset{\text{---}}{\underset{\circ}{\text{---}}} \text{---} + \mathcal{O}(\nu^3). \end{aligned} \quad (2)$$

Steady-state density and current. In the present work we focus on the steady state,

Suppl. C. We write the steady-state density ρ_+ of right-moving particles as a power series in ν^n with coefficients $\rho_+^{(n)}$,

$$\begin{aligned} \rho_+(x) &= \sum_{n=0}^{\infty} \nu^n \rho_+^{(n)}(x) \\ &= \lim_{t_0 \rightarrow -\infty} \left\langle \phi(x, t) \tilde{\phi}(x_0, t_0) \right\rangle \end{aligned} \quad (3)$$

and similarly for the density of left moving particles ρ_- , so that $\rho(x) = \rho_+(x) + \rho_-(x)$. For finite tumble rate γ , the steady-state densities ρ_{\pm} are independent of the initial state. As discussed in Suppl. C, the limit $t_0 \rightarrow -\infty$ effectively amputates the right, incoming leg in the diagrams, Eq. (2), so that they readily provide us with a diagrammatic expansion of the steady state density, order by order in ν .

Calculating the a th Fourier coefficient $\rho_a^{(n)}$ of the steady-state density ρ to order n in ν is now a matter of some well-organised algebra (Suppl. C). To this end, we introduce the polarity $\mu(x) = \rho_+(x) - \rho_-(x)$ and express the steady-state current as

$$J = w\mu(x) - (D\partial_x + \nu U'(x))\rho(x). \quad (4)$$

Defining the matrix (Suppl. C 2 a)

$$\underline{\underline{M}}_a = \frac{k_a \mathcal{I}_a}{\Gamma_a^0 \Gamma_{-a}^0 - \gamma^2} \begin{pmatrix} -Dk_a^2 + 2\gamma & iwk_a \\ iwk_a & -Dk_a^2 \end{pmatrix} \quad (5)$$

with $\Gamma_a^0 = \Gamma_a(0; 0) = Dk_a^2 - iwk_a + \gamma$, Eq. (B16), and $\mathcal{I}_a = 1 - \delta_{a,0}$, Eq. (C9), the density and the polarity at order n in ν are the elements of the vector

$$\begin{pmatrix} \rho_{a_1}^{(n)} \\ \mu_{a_1}^{(n)} \end{pmatrix} = \sum_{a_2, \dots, a_n} W_{a_1 - a_2} W_{a_2 - a_3} \cdots W_{a_{n-1} - a_n} W_{a_n} \underline{\underline{M}}_{a_1} \underline{\underline{M}}_{a_2} \cdots \underline{\underline{M}}_{a_n} \begin{pmatrix} 1 \\ 0 \end{pmatrix} \quad (6)$$

with $W_a = U_a k_a / L$. Using Eq. (4), the steady-state current at order n in ν is correspondingly

$$J^{(n)} = -\frac{i}{L} \sum_{a_1, \dots, a_{n-1}} W_{-a_1} W_{a_1 - a_2} W_{a_2 - a_3} \cdots W_{a_{n-2} - a_{n-1}} W_{a_{n-1}} \begin{pmatrix} 1 \\ 0 \end{pmatrix}^\top \underline{\underline{M}}_{a_1} \underline{\underline{M}}_{a_2} \cdots \underline{\underline{M}}_{a_{n-1}} \begin{pmatrix} 1 \\ 0 \end{pmatrix}. \quad (7)$$

This concludes our derivation. Calculating the current is now a matter of performing the matrix multiplications and summation in Eq. (7)

for a potential given in terms of its modes U_a and summing these contributions order by or-

der in ν , so that

$$J = \sum_{n=0}^{\infty} \nu^n J^{(n)}. \quad (8)$$

From the symmetries of \underline{M}_a , Eq. (5), and the form of Eq. (7), it follows that there is no current to first order in ν and generally no contributions to the steady-state current in even powers of ν , Suppl. E1. As a result, the current reverts if the potential is inverted, $U \rightarrow -U$. This is not a trivial insight, because the steady-state *density* of the inverted potential generally bears no resemblance to that of the original potential, Fig. E1, which may have been overlooked [34]. Several other properties of the steady-state current J arising from Eq. (8) are discussed in detail in Suppl. C. Firstly, in a potential even about x^* , *i.e.* $U(x^* + x) = U(x^* - x)$, the steady-state current, of course, vanishes, because the potential fails to provide even just a preferred direction [35], Suppl. E3. The steady-state current also vanishes if the potential $U(x)$ has only odd modes, *i.e.* $U_a = 0$ for all even a , which renders it “supersymmetric” [34], $U(x) = -U(x + L/2)$, Suppl. E2.

The steady-state current in any potential parameterised by U_a is given by Eqs. (7) and (8). Any numerical scheme can cope only with a finite number of modes, as the sums in Eq. (7) need to terminate, and similarly for the maximum order of ν entering in Eq. (8). Nevertheless, including hundreds of modes to calculate the current to hundreds of orders in ν , in principle poses little numerical difficulty. To confirm the correctness of our scheme, we calculate the current for a plain ratchet and compare to [4], which can be done to large extent in closed form, Suppl. D, owing to the piece-wise linearity of the potential. Fig. D2 demonstrates perfect agreement of the steady-state current calculated in both schemes for all $\nu < \nu_{\text{roc}}^<$. Beyond that point the power series Eq. (8) eventually diverges. In principle, the radius of convergence ν_{roc} is determined, say, through the root test on the odd terms of the series Eq. (8), $\nu_{\text{roc}} = 1/\limsup_{m \rightarrow \infty} |J^{(2m+1)}|^{1/(2m+1)}$, but in the present numerical procedures based on gradient descent, we used the more conservative estimate of the minimal radius of convergence of the derivative of Eq. (8),

$$\nu_{\text{roc}}^< = \min \left(|m J^{(m)}|^{-\frac{1}{m-1}} : m = 3, 5, \dots, n \right), \quad (9)$$

with n the highest order calculated.

Optimising the potential. The current Eq. (8) picks up as ν^3 , but eventually falters

as ν becomes so large that νU is too steep for the self-propulsion speed to overcome the potential. Somewhere in-between lies the *optimal potential that maximises the current*, passable for the RnT particles in one direction, but (almost) impassable in the other direction.

To find the best such *shape*, we fix $\nu = 1$, rendering $\Phi(x)$ equal to $U(x)$ for the remainder of this section, and, leaving ν untouched, instead we find the modes U_a that maximise the steady-state current J , Eqs. (7) and (8), using `frprmn` [36], Suppl. A1. Once such an “optimal potential” $\widehat{U}(D, w, L, \gamma; x)$ as a function of the parameters is found in terms of its modes \widehat{U}_a , we determine its current \widehat{J} for this potential, as well as, *a posteriori*, its radius of convergence $\widehat{\nu}_{\text{roc}}$ according to Eq. (9), to confirm that it exceeds unity. Since $U(x)$ is real, $U_a^* = U_{-a}$, each pair (U_a, U_{-a}) may be written as an amplitude and a phase. To avoid degeneracy, we further fix the phase of the lowest mode so that U_1 is purely imaginary. Further, we de-dimensionalise the problem, leaving only two parameters, the Péclet number $Pe = wL/D$ and $Qe = \gamma L^2/D$. In this parameterisation, length is measured in units of L , diffusion and the potential in units of D and time therefore in units of L^2/D . We think in the following of L and D as being fixed, so that Pe parameterises the self-propulsion velocity, Qe the tumbling rate and $\widehat{U}(D, w, L, \gamma; x) = D\widehat{U}(1, Pe, 1, Qe; x/L)$. While any particular choice of the underlying parameterisation should make no difference to the optimisation scheme, making different choices for D, w, L and γ for the same Pe and Qe gives us a way to overcome some practical, numerical limitations.

Results. The resulting shape of the optimal potential is surprisingly stable across the range of Pe and Qe explored. Fig. 1 shows a typical shape, Fig. 2 shows two more for somewhat more extreme parameter values. The shape resembles that of the letter N, but it is not a simple, piece-wise linear ratchet. The resulting current in the figures above takes place from left to right. The deep crevasse towards $x = 0$ in Fig. 1, towards the left followed by a steep rise of the potential towards the left and over to the right by periodicity, traps particles and prevents them from moving left. There is always a shallower path towards the right, that terminates in a sharp peak towards $x = L$, rendering the whole shape inversion symmetric about $(L/2, 0)$. An apparent discontinuity at $x = 0$ results in the Gibbs phenomenon, Suppl. A2.

The Péclet-number Pe indicates whether *free* particle movement is dominated by diffusion,

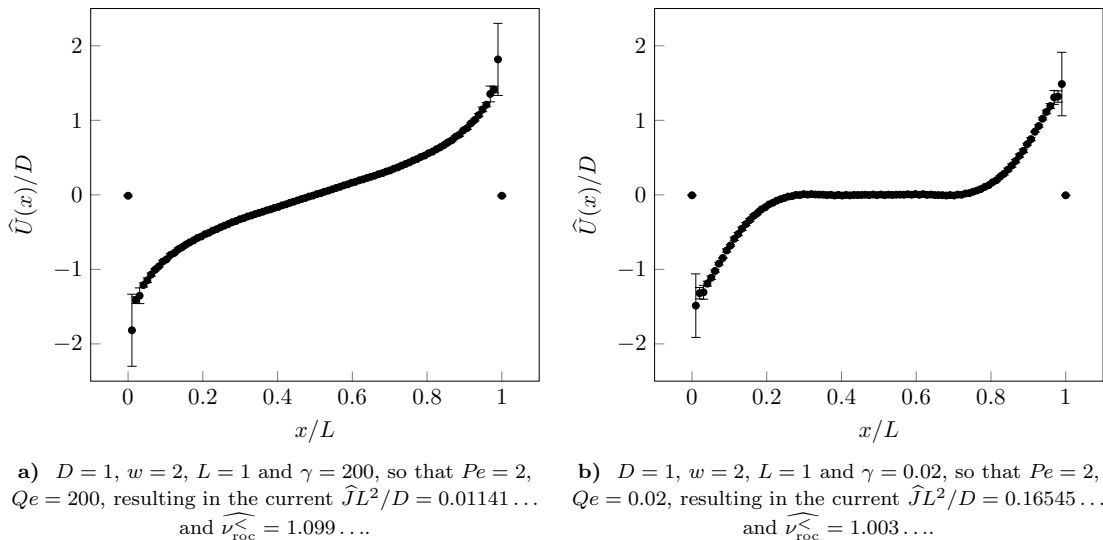


FIG. 2: Shapes of potential maximising the steady-state current at the parameter values indicated. Technical details of the plots in Suppl. A 2.

$Pe < 1$, or ballistic motion, $Pe > 1$. The additional complications of tumbling and potential modify its rôle. On the large scale, diffusion is enhanced by $L\gamma^2$. On the small scale, diffusion D sets the scale of the maximum barrier height the particle can overcome. Without potential, ballistic transport dominates on the scale of the system, if $w/\gamma > L$, *i.e.* $\kappa = Pe/Qe > 1$.

To rectify the flow optimally, the basic design principles we derive from Figs. 1 and 2 are, firstly, the need for a deep crevasse, Fig. 1, to set a high hurdle to a RnT particle attempting to pass through the potential towards the left. Similarly, a sharp peak at around $x = L$ increases the barrier height. The rise of the potential required as a barrier grows linearly in D . The second design principle is the shallower incline of the potential towards the right, where the potential difference of the steep crevasse is spread out across the whole length L of the potential, making it much less of an obstacle for particle movement towards the right.

Apart from the deep crevasse and the sharp peak on either end of the shallow incline, the intermediate “plane”, Fig. 1, may be expected to have a slope of around w , so that it is just about overcome by a right-moving RnT particle. However, for this long section to be passed *ballistically* within time $1/\gamma$, its slope would have to be less than $w - L\gamma$. This can be realised only when w is sufficiently large, as the slope is necessarily positive. If ballistic transport dominates over diffusion, $Pe > 1$, but ballistic transport itself is too slow to overcome any significant potential slope within the time available

between tumbles, $\kappa = Pe/Qe = w/(L\gamma) \ll 1$, we expect a flat plane maximising the steady-state current. Together with the need of a high barrier around $x = 0$, $Pe > 1$ and $Qe \gg 1$ result in sharp crevasses and peaks, Fig. 2a.

If, on the other hand, ballistic transport is strong, $\kappa > 1$ and $Pe > 1$, the slope of the potential in the plane is not constrained by the ballistic transport but rather by the need to connect (only) between the bottom and the top of the barrier face, *i.e.* the slope will scale like D/L . In this case, $Pe > 1$ and $Qe \ll 1$, the intermediate slope is steeper and the crevasses widened, Fig. 2b, producing a relatively large current.

If transport is primarily diffusive, $Pe < 1$, large $Qe = \gamma L^2/D$ effectively enhances the diffusion on spatial scales greater than w/γ . Transport in this parameter region is typically poor.

In general, a high barrier helps rectify the steady-state current. The need for a high barrier requires potential differences so large, that the slope of the potential $\propto D/L$ in the plane exceeds the self-propulsion velocity w . This phenomenon can be observed already in a piecewise linear ratchet with the steady-state current J plotted in Fig. D2, where the maximum current is attained when the slope of the long “plane” section is around $3.9/0.9$, far exceeding the self-propulsion velocity of $w = 1$.

The periodic nature of the setup allows for any $\widehat{U}(D, w, L, \gamma; x)$ to be periodically repeated ℓ times and investigated as a candidate for the optimal potential $\widehat{U}(D, w, \ell L, \gamma; x)$.

Such a potential would have only modes U_ℓ , $U_{2\ell}$ populated with all other modes $\widehat{U}_1, \dots, \widehat{U}_{\ell-1}, \widehat{U}_{\ell+1}, \dots$ vanishing, as the first mode of $\widehat{U}(\dots, L, \dots)$ gets mapped to the ℓ th mode of $\widehat{U}(\dots, \ell L, \dots)$, the second to the 2ℓ -th mode and so on. This consideration provides the lower bound $\widehat{J}(D, w, \ell L, \gamma) \geq \widehat{J}(D, w, L, \gamma)/\ell$ as the steady-state current of the ℓ -fold repeat of the potential is an ℓ th of the original, and thus

$$\widehat{J}(1, \ell Pe, 1, \ell^2 Qe) \geq \ell \widehat{J}(1, Pe, 1, Qe). \quad (10)$$

Discussion. The optimal rectified current \widehat{J} is generally small compared to the unidirectional current w/L . Only for $Pe \rightarrow \infty$ and $Qe \downarrow 0$ the particles whizz through the potential in one direction, getting stuck on any tiny snag of a conventional ratchet in the other, so that $\widehat{J} = (1/2)w/L$. A key question to address in future research is whether an external potential provides the best rectification or whether there are other passive devices that do a better job. What are the limits of rectification?

An experimental verification of our work requires a fine-tuned potential landscape. Microorganisms have been subjected to a potential well by optical trapping [37], bidirectional molecular motors by magnetic trapping [38], but simpler effective potential, due to boundary interaction [39, 40] and a transversal microfluidic flow may be equally feasible.

Typical values for *E. coli* are $D = 0.2 \mu\text{m}^2/\text{s}$ for the thermal diffusion constant, $w = 40 \mu\text{m}/\text{s}$ for the self-propulsion speed and $\gamma = 1\text{s}^{-1}$ for the tumble rate [41, 42], producing values between $Pe = 1000$ and $Qe = 125$ for $L = 5 \mu\text{m}$ and $Pe = 2 \cdot 10^4$ and $Qe = 5 \cdot 10^4$

for $L = 100 \mu\text{m}$. For these parameters we expect the optimal potential to be akin to Fig. 2a. Because the radius of convergence drops significantly with increasing Peclet number, we are not able to determine the shape directly.

The field theoretic formalism above can be extended: Firstly, it provides a route to the steady-state entropy production via Gaspard's [43, 44] approach, which, however, lies beyond the scope of the present work. While it is fairly straight-forward to calculate it for the full Markov process, determining it while ignoring the particle species is notoriously difficult [45]. One might expect, however, that maximised current coincides with maximised entropy production. Secondly, the lack of convergence as shown in Fig. D2 for $\nu > \nu_{\text{roc}}^<$ is a challenge that needs to be overcome, possibly with the help of renormalisation. Thirdly, although many experimental settings are well captured in one longitudinal and one transversal spatial dimension, extending the present framework to two dimension plus one transversal direction is an important generalisation.

This work determines the properties of the potential that optimally rectifies the steady-state current of RnT particles. We have shown that generally, the profile deviates significantly from an ordinary ratchet. Our quantitative and qualitative findings provide the design principles for rectification devices for microorganisms and for the cogs and wheels of an active engine [46].

Acknowledgements We thank Martin Bier for helpful discussions and acknowledge communications with Peter Reimann. ZZ thanks Huiyao Zheng for technical support.

-
- [1] M. C. Marchetti, J. F. Joanny, S. Ramaswamy, T. B. Liverpool, J. Prost, M. Rao, and R. A. Simha, *Rev. Mod. Phys.* **85**, 1143 (2013).
 - [2] C. R. Doering and J. C. Gadoua, *Phys. Rev. Lett.* **69**, 2318 (1992).
 - [3] M. O. Magnasco, *Phys. Rev. Lett.* **71**, 1477 (1993).
 - [4] R. D. Astumian and M. Bier, *Phys. Rev. Lett.* **72**, 1766 (1994).
 - [5] G. A. Pavliotis, *Phys. Lett. A* **344**, 331 (2005).
 - [6] P. Galajda, J. Keymer, P. Chaikin, and R. Austin, *J. Bacteriol.* **189**, 8704 (2007), 17890308.
 - [7] D. Martin, J. O'Byrne, M. E. Cates, É. Fodor, C. Nardini, J. Tailleur, and F. van Wijland, *Phys. Rev. E* **103**, 032607 (2021).
 - [8] L. Angelani, A. Costanzo, and R. Di Leonardo, *EPL* **96**, 68002 (2011).
 - [9] Y. Baek, A multiscale approach to Brownian motors (2019), private communication.
 - [10] L. Angelani, R. Di Leonardo, and G. Ruocco, *Phys. Rev. Lett.* **102**, 048104 (2009).
 - [11] N. Koumakis, C. Maggi, and R. Di Leonardo, *Soft Matter* **10**, 5695 (2014).
 - [12] R. Di Leonardo, L. Angelani, D. Dell'Arciprete, G. Ruocco, V. Iebba, S. Schippa, M. P. Conte, F. Mecarini, F. De Angelis, and E. Di Fabrizio, *Proc. Natl. Acad. Sci. U.S.A.* **107**, 9541 (2010).
 - [13] L. Berthier and J. Kurchan, *Nat. Phys.* **9**, 310 (2013).
 - [14] P. S. Hagan, C. R. Doering, and C. D. Levermore, *SIAM J. Appl. Math.* **49**, 1480 (1989).

- [15] B. Lindner, M. Kostur, and L. Schimansky-Geier, *Fluct. Noise Lett.* **01**, R25 (2001).
- [16] P. K. Ghosh, V. R. Misko, F. Marchesoni, and F. Nori, *Phys. Rev. Lett.* **110**, 268301 (2013).
- [17] P. C. Bressloff and J. M. Newby, *Rev. Mod. Phys.* **85**, 135 (2013).
- [18] H. Brenner, *Langmuir* **6**, 1715 (1990).
- [19] E. Woillez, Y. Zhao, Y. Kafri, V. Lecomte, and J. Tailleur, *Phys. Rev. Lett.* **122**, 258001 (2019).
- [20] B. Bijnens and C. Maes, *J. Stat. Mech.: Theory Exp.* **2021** (3), 033206.
- [21] B. Walter, G. Pruessner, and G. Salbreux, *Phys. Rev. Res.* **3**, 013075 (2021).
- [22] E. Tjhung, C. Nardini, and M. E. Cates, *Phys. Rev. X* **8**, 031080 (2018).
- [23] F. Berger, T. Schmiedl, and U. Seifert, *Phys. Rev. E* **79**, 031118 (2009).
- [24] J. Tailleur and M. E. Cates, *Phys. Rev. Lett.* **100**, 218103 (2008).
- [25] Z. Zhang and G. Pruessner, *arXiv* (2021), 2106.07383.
- [26] R. Feynman, R. Leighton, and M. Sands, *The Feynman Lecturers in Physics* (Addison-Wesley, Reading, 1963).
- [27] M. E. Cates, *Rep. Prog. Phys.* **75**, 042601 (2012).
- [28] S. Coppola and V. Kantsler, *Phys. Rev. E* **104**, 014602 (2021).
- [29] M. Doi, *J. Phys. A: Math. Gen.* **9**, 1465 (1976).
- [30] L. Peliti, *J. Phys.* **46**, 1469 (1985).
- [31] J. Cardy, G. Falkovich, and K. Gawedzki, *Non-equilibrium Statistical Mechanics and Turbulence* (Cambridge University Press, Cambridge, England, UK, 2008).
- [32] U. C. Täuber, *Critical Dynamics: A Field Theory Approach to Equilibrium and Non-Equilibrium Scaling Behavior* (Cambridge University Press, Cambridge, England, UK, 2014).
- [33] R. Garcia-Millan and G. Pruessner, To be published (2022).
- [34] P. Reimann, *Phys. Rev. Lett.* **86**, 4992 (2001).
- [35] N. Razin, *Phys. Rev. E* **102**, 030103 (2020).
- [36] W. H. Press, S. A. Teukolsky, W. T. Vetterling, and B. P. Flannery, *Numerical Recipes* (Cambridge University Press, Cambridge, England, UK, 2007).
- [37] H. Xin, Q. Liu, and B. Li, *Sci. Rep.* **4**, 1 (2014).
- [38] T. Fallesen, J. Roostalu, C. Duellberg, G. Pruessner, and T. Surrey, *Biophys. J.* **113**, 2055 (2017), 29117528.
- [39] G. Vizsnyiczai, G. Frangipane, S. Bianchi, F. Saglimbeni, D. Dell’Arciprete, and R. Di Leonardo, *Nat. Commun.* **11**, 1 (2020).
- [40] O. Sipos, K. Nagy, R. Di Leonardo, and P. Galajda, *Phys. Rev. Lett.* **114**, 258104 (2015).
- [41] J. Singh, A. E. Patteson, P. K. Purohit, and P. E. Arratia, *arXiv* (2017), 1710.04068.
- [42] O. T. Dyer and R. C. Ball, *Phys. Fluids* **33**, 051904 (2021).
- [43] P. Gaspard, *J. Stat. Phys.* **117**, 599 (2004).
- [44] L. Cocconi, R. Garcia-Millan, Z. Zhen, B. Buturca, and G. Pruessner, *Entropy* **22**, 1252 (2020).
- [45] R. Garcia-Millan and G. Pruessner, *J. Stat. Mech.: Theory Exp.* **2021** (6), 063203.
- [46] P. Pietzonka, É. Fodor, C. Lohrmann, M. E. Cates, and U. Seifert, *Phys. Rev. X* **9**, 041032 (2019).
- [47] J. W. Gibbs, *Nature* **59**, 200 (1898).
- [48] U. C. Täuber, M. Howard, and B. P. Vollmayr-Lee, *J. Phys. A: Math. Gen.* **38**, R79 (2005).
- [49] W. R. Inc., *Mathematica*, Version 13.0.0 (2021), champaign, IL, 2021.

Appendix A: Numerical optimisation and plotting procedure

In this section, we discuss the numerical procedures employed to determine the optimal shape $\widehat{U}(x)$ of the potential and to subsequently generate the plots of the potential $U(x)$ in Figs. 1 and 2. The optimisation scheme outlined in the main text results in the potential being characterised by its modes U_a and translating a finite number of them to a potential $U(x)$ in real space is marred by ambiguity. We will outline the process of generating the plots, the origin of the error bars, the Gibbs phenomenon and the resolution of troughs and peaks.

1. Optimisation procedure

In the following we outline the numerical procedure to determine the optimal potential $\widehat{U}(x)$, *i.e.* the potential that maximises the steady-state current J . The numerical scheme draws on Eqs. (7) and (8), which effectively produce the steady-state current J for any given, finite set of $2A + 1$ modes of the potential U_a with $a = -A, -A + 1, \dots, A$. The numerical scheme is greatly improved by expressing the partial derivative of J with respect to any of the modes U_a . While tedious to determine, given the structure of Eq. (7), a closed-form expression is readily available.

While the finite number of modes, $2A + 1$, limits the summation to be performed in Eq. (7), the order of ν needs to be limited to \mathcal{N}_ν in the sum Eq. (8).

As $U(x)$ is real, the modes U_a are complex conjugate pairs, $U_a^* = U_{-a}$. The 0-mode U_0 does not enter at all, so that for any given A the maximisation scheme determines A complex numbers, U_a with $a = 1, 2, \dots, A$.

If $\widehat{U}(x)$ extremises the current, so does $\widehat{U}(L-x)$ and in fact any translation of the two, $\widehat{U}(x^* \pm x)$. To break symmetry, we demand U_1 be purely imaginary, leaving the maximisation scheme with $2A - 1$ degrees of freedom. We found that generally the maximisation scheme is not sensitive to the details of the initialisation. We have also verified that the maximum current is not obtained with periodically repeated potentials, “higher harmonics”, where only modes are populated that are multiples of some a^* , *i.e.* $U_{a^*}, U_{2a^*}, U_{3a^*}$ are non-zero and all other modes vanish.

We found numerically that the steady-state current is maximised if all U_a are purely imaginary up to a small numerical error. As a result the optimal potential obeys $\widehat{U}(L/2 + x) = -\widehat{U}(L/2 - x)$. Demanding this throughout the maximisation scheme reduces the degrees of freedom to A , without changing the optimal shape $\widehat{U}(x)$ or the optimal current \widehat{J} .

We used `frprmn` [36] to obtain the results reported in the present work. The following heuristic proved efficient:

0. Initialisation: $A = 50$, $\mathcal{N}_\nu = 75$ and U_a for $a = -50, -49, \dots, 50$ are initialised with $U_a = i/(2\pi a)$, which are the Fourier coefficients of a piece-wise periodic linear ratchet $U(x) = x$ for $x \in [0, L)$.
1. Given the other parameters, D, w, L, γ , as well as Eqs. (7) and (8) with the sum running up to \mathcal{N}_ν , the optimal \widehat{U}_a are determined using `frprmn` [36].
2. The results are written into a file and A is increased by 50. These additional degrees of freedom are initialised with 0. Those determined so far serve as initial values for the optimisation with increased A . The procedure returns to step 1.

Throughout the optimisation procedure, we determine the apparent radius of convergence of the power series Eq. (8) as the value of $(J^{(n)})^{-1/n}$ for the largest (odd) n that produces a finite numerical value. If the optimisation procedure strays into a parameter region where this radius of convergence drops below unity, the supposed current becomes numerically unreliable. In this case, the optimisation is considered unattainable within the present perturbative framework and the optimisation is abandoned, *i.e.* we do not pursue the optimisation for these parameter values further and no results are shown in the present work. If, on the other hand, an optimal potential $\widehat{U}(x)$ is eventually found, we also determine the radius of convergence $\widehat{\nu}_{\text{roc}}^<$, Eq. (9), *a posteriori* to ensure that it is greater than unity.

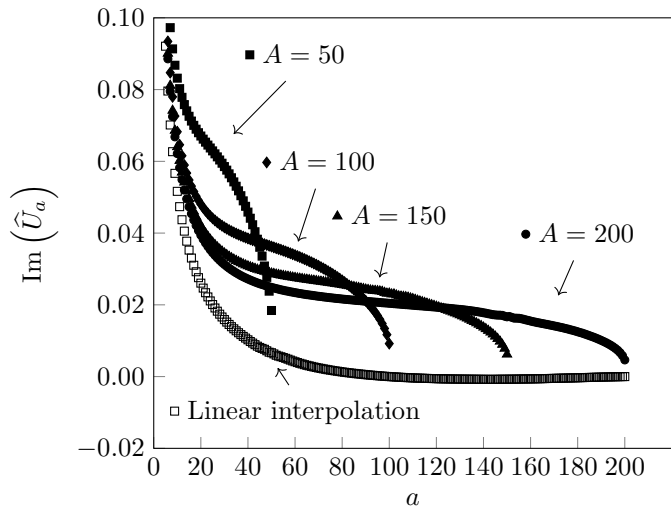


FIG. A1: Imaginary part of the modes \hat{U}_a allowing for $A = 50, 100, 150, 200$ modes in the optimisation procedures (filled symbols) and, also, as extracted from the linear interpolation of the potential shown in Fig. 1 (open squares). Parameters are $D = 1$, $w = 1$, $L = 1$ and $\gamma = 1$, so that $Pe = Qe = \kappa = 1$.

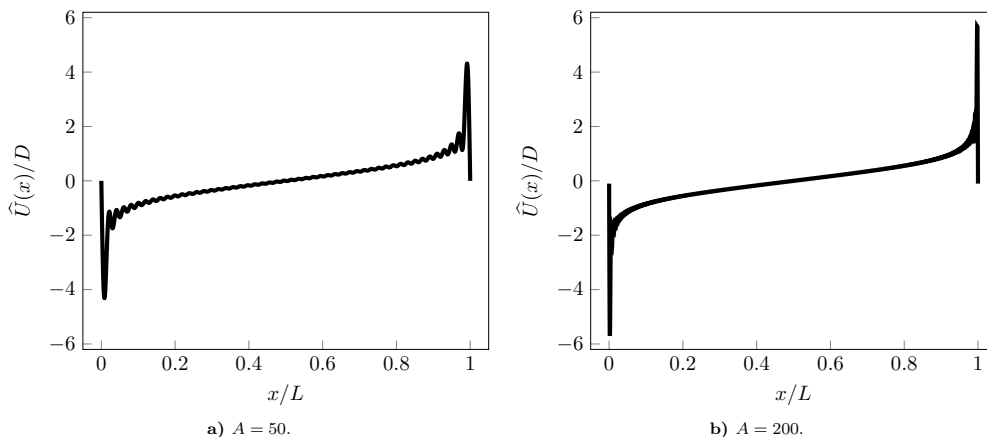


FIG. A2: The optimal potential $\hat{U}(x)$ of Fig. 1 shown with higher resolution of 2000 points and $A = 50, 200$ as indicated. The peaks around $x = 0$ and $x = L$ are likely to be artefacts, as discussed in the text.

2. Plotting procedure

The plots Figs. 1 and 2 are generated as follows. With $\mathcal{N}_\nu = 75$ the modes \hat{U}_a are determined for $A = 100$, $A = 150$ and $A = 200$. Increasing A gives the optimisation procedure more degrees of freedom, which affects *all* modes, *e.g.* in general, \hat{U}_a determined with $A = 100$ differs from \hat{U}_a determined with $A = 150$ for all a , in particular at $a \leq 100$. Fig. A1 shows how \hat{U}_a changes with A , with the largest (relative) change visible for a close to A , whereas \hat{U}_a for smaller a suggest convergence.

Evaluating Eq. (B11) in the form

$$\hat{U}(x) = \frac{1}{L} \sum_{a=-A}^A e^{ik_a x} \hat{U}_a \quad (\text{A1})$$

at numerically densely chosen positions x reveals an apparent undulation throughout and turning into some distinct peaks close to $x = 0$ and $x = L$ reminiscent of the Gibbs phenomenon [47], Fig. A2. The problem persists even at large A , although the undulations away from $x = 0, L$

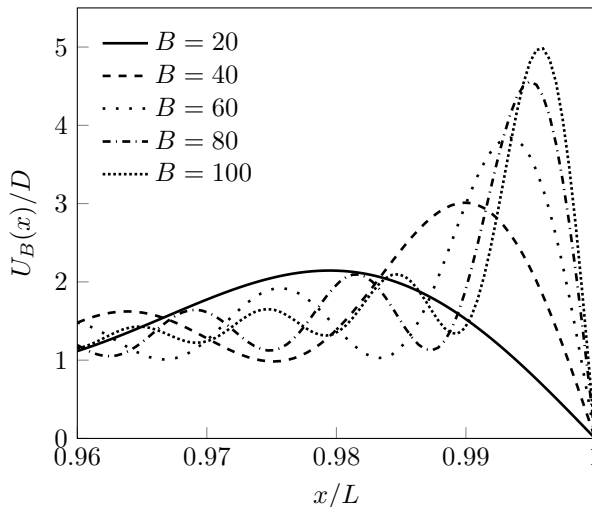


FIG. A3: Detail of the potential $U_B(x)/D$ of Eq. (A2) around the peak near $x/L = 1$ based on $A = 100$ modes using $B = 20, 40, 60, 80$ and 100 modes respectively in the sum. Parameters: $D = 1$, $w = 1$, $L = 1$ and $\gamma = 1$, so that $Pe = Qe = \kappa = 1$.

become less noticeable.

This is confirmed in a modified sum,

$$U_B(x) = \frac{1}{L} \sum_{a=-B}^B e^{ik_a x} \widehat{U}_a \quad (\text{A2})$$

where the summation runs only over $B \leq A$ modes, *i.e.* it takes into account fewer modes in the plot than are available in the given numerical optimisation of the first A modes. As shown in Fig. A3, the resulting sharp peaks around $x = 0$ and $x = L$ are present even for moderate values of B , although they, of course, change shape. This suggests that their presence in Fig. A2 is not due to the relatively big error of \widehat{U}_a at a around A , but due to the Gibbs phenomenon, which arises when a Fourier-sum of a discontinuous function is terminated after finitely many terms, even when the infinite sum is exact. In other words, some features around $x = 0$ and $x = L$ are not due to poor numerical estimates of \widehat{U}_a as A is finite, but instead caused by the Gibbs phenomenon, *i.e.* using a finite number of modes to describe a discontinuous function.

The plots shown in Figs. 1 and 2 are designed to show what we know about the potential $\widehat{U}(x)$ and quantify its convergence. To achieve this, we determine the modes of the best potential for $A = 100$, $A = 150$ and $A = 200$ and evaluate Eq. (A1) at values of x incommensurate with all L/A in an attempt to avoid “resonances” and with spacing greater than the largest L/A . In Figs. 1 and 2 we choose x at multiples of $L/97$. The error bars in these plots indicate the range of $\widehat{U}(x)$ for the different A at the corresponding x . This procedure avoids artefacts due to the Gibbs phenomenon at $x = 0$ and $x = L$ as well as the undulations throughout finite A . However, given the comparative sparseness of the points, sharp features are not well resolved, in particular those close to $x = 0$ and $x = L$.

One might be tempted to linearly interpolate the points in the resulting plots, say Fig. 1. However, as shown in Fig. A1, determining the resulting modes U_a by Fourier-transform of such a linear interpolation, shows that they are generally a very poor match with the modes that gave rise to the plot in the first place, even when their inverse Fourier transform reproduces Fig. 1 perfectly. Only the very low modes up to $|a| = 5$ agree within 10%. As a result, the current of 200 such modes produces only $JL^2/D = 0.01872\dots$, and is thus reduced by a factor 0.5 compared to the optimal current obtained originally.

The plotting procedure used in the main text thus provides a useful representation of the potential in real space with suitable indication of how reliably we have determined certain features. The ambiguity arises because the optimisation procedure produces modes, as shown in Fig. A1 rather than an estimate of the shape in real space.

Appendix B: Field theory

In this section, we give a derivation of the path-integral formulation of RnT motion in a periodic potential using Doi-Peliti field theory. The coupled Fokker-Planck equations describing an RnT particle in a periodic potential $\nu U(x)$ are, similar to Eqs. (D2),

$$\begin{aligned}\partial_t \rho_+(x, t) &= -\partial_x[(w - \nu U'(x))\rho_+(x, t)] - \gamma(\rho_+(x, t) - \rho_-(x, t)) + D\partial_x^2 \rho_+(x, t) \\ \partial_t \rho_-(x, t) &= -\partial_x[(-w - \nu U'(x))\rho_-(x, t)] - \gamma(\rho_-(x, t) - \rho_+(x, t)) + D\partial_x^2 \rho_-(x, t)\end{aligned}\quad (\text{B1a})$$

where $\rho_+(x, t)$ and $\rho_-(x, t)$ are the densities of right-moving and left-moving particles respectively, as a function of the position x and time t . The dashed potential $U'(x)$ denotes its derivative. We further introduce the total particle density $\rho(x, t) = \rho_+(x, t) + \rho_-(x, t)$ and the polarity $\mu(x, t) = \rho_+(x, t) - \rho_-(x, t)$, so that the particle current

$$J(x, t) = (w - \nu U'(x) - D\partial_x)\rho_+(x, t) + (-w - \nu U'(x) - D\partial_x)\rho_-(x, t) \quad (\text{B2})$$

can be re-written as

$$J(x, t) = w\mu(x, t) - \rho(x, t)\nu U'(x) - D\partial_x \rho(x, t) \quad (\text{B3})$$

and the Fokker-Planck equation as

$$\begin{aligned}\partial_t \rho(x, t) &= -\partial_x[w\mu(x, t) - \rho(x, t)\nu U'(x) - D\partial_x] = -\partial_x J(x, t) \\ \partial_t \mu(x, t) &= -\partial_x[w\rho(x, t) - \mu(x, t)\nu U'(x)] - 2\gamma\mu(x, t) + D\partial_x^2 \mu(x, t).\end{aligned}\quad (\text{B4})$$

The Fokker-Planck equation describes the evolution of a particle density. *A priori*, it does not enforce the particle entity of the constituent degrees of freedom, nor is it concerned with it — the *densities* ρ_{\pm} above are completely unconstrained by being due to particles and could equally describe, say, a temperature profile. To cast it into a Doi-Peliti field theory, the Fokker-Planck equation is normally re-written as a master equation by discretising space and interpreting it as the evolution of the *probability (density)* of finding a *single particle* at a particular position, before generalising it to the evolution of *multiple, indistinguishable particles* and the probability of obtaining a particular *occupation number configuration*. In the canonical procedure [31, 48] the field-theoretic action is then obtained by expressing the evolution in terms of ladder operators, turning them into conjugate fields and taking the continuum limit. This procedure invariably reproduces the Fokker-Planck operator in the action \mathcal{A} [33], which after rearranging can be expressed as the sum $\mathcal{A} = \mathcal{A}_0 + \mathcal{A}_1$ of a harmonic part

$$\begin{aligned}\mathcal{A}_0 &= \int_0^L dx \int dt \tilde{\phi}(x, t)(\partial_t + w\partial_x - D\partial_x^2 + r)\phi(x, t) + \tilde{\psi}(x, t)(\partial_t - w\partial_x - D\partial_x^2 + r)\psi(x, t) \\ &\quad + \gamma(\tilde{\phi}(x, t) - \tilde{\psi}(x, t))(\phi(x, t) - \psi(x, t))\end{aligned}\quad (\text{B5})$$

and a perturbative part,

$$\mathcal{A}_1 = \int_0^L dx \int dt \nu(\partial_x \tilde{\phi}(x, t))U'(x)\phi(x, t) + \nu(\partial_x \tilde{\psi}(x, t))U'(x)\psi(x, t) \quad (\text{B6})$$

where $\phi(x, t)$ and $\psi(x, t)$ are the annihilation fields of a right-moving and a left-moving particle respectively and $\tilde{\phi}(x, t)$ and $\tilde{\psi}(x, t)$ are, correspondingly, the Doi-shifted [31] creation fields of a right-moving and a left-moving particle so that $\phi^\dagger = \tilde{\phi} + 1$ and $\psi^\dagger = \tilde{\psi} + 1$. We have included in the harmonic part a positive *mass* r as to regularise the infrared and restore causality. The mass is a mere technicality and will be taken to 0^+ whenever suitable. The perturbative part of the action \mathcal{A}_1 in Eq. (B6) incorporates the perturbative parameter ν in front of the potential $U(x)$ to guide the perturbation theory that is to follow.

The expectation of an observable in terms of fields is taken via the path-integral [45]

$$\langle \bullet \rangle = \int \mathcal{D}[\phi, \tilde{\phi}, \psi, \tilde{\psi}] \bullet e^{-\mathcal{A}[\phi, \tilde{\phi}, \psi, \tilde{\psi}]} . \quad (\text{B7})$$

Only at $\nu = 0$ this path integral can generally be taken in closed form,

$$\langle \bullet \rangle_0 = \int \mathcal{D}[\phi, \tilde{\phi}, \psi, \tilde{\psi}] \bullet e^{-\mathcal{A}_0[\phi, \tilde{\phi}, \psi, \tilde{\psi}]} \quad (\text{B8})$$

about which the action in the perturbative part is expanded, so that

$$\langle \bullet \rangle = \sum_{n=0}^{\infty} \frac{1}{n!} \langle \bullet (-\mathcal{A}_1)^n \rangle_0 . \quad (\text{B9})$$

To make the action local in the fields, we introduce a Fourier representation in the form

$$\phi(x, t) = \frac{1}{L} \sum_{a=-\infty}^{\infty} e^{ik_a x} \int_{-\infty}^{\infty} d\omega e^{-i\omega t} \phi_a(\omega) \quad (\text{B10})$$

and correspondingly for all other fields and observables, with $d\omega = d\omega/(2\pi)$ and $k_a = 2\pi a/L$, which readily accommodates the periodic nature of x . For example the potential in real space is expressed as

$$U(x) = \frac{1}{L} \sum_{a=-\infty}^{\infty} e^{ik_a x} U_a \quad \text{with} \quad U_a = \int_0^L dx e^{-ik_a x} U(x) \quad (\text{B11})$$

in terms of its *modes* or coefficients U_a .

The bare propagators are easily determined from Eq. (B5) in the form

$$\mathcal{A}_0 = \frac{1}{L} \sum_a \int d\omega \begin{pmatrix} \tilde{\phi}_{-a}(-\omega) \\ \tilde{\psi}_{-a}(-\omega) \end{pmatrix}^{\top} \underline{\underline{A}}_a(\omega) \begin{pmatrix} \tilde{\phi}_a(\omega) \\ \tilde{\psi}_a(\omega) \end{pmatrix} \quad (\text{B12})$$

with

$$\underline{\underline{A}}_a(\omega) = \begin{pmatrix} -i\omega + Dk_a^2 + i\omega k_a + r + \gamma & -\gamma \\ -\gamma & -i\omega + Dk_a^2 - i\omega k_a + r + \gamma \end{pmatrix} \quad (\text{B13})$$

by calculating the inverse

$$\left(\underline{\underline{A}}_a(\omega) \right)^{-1} \delta(\omega + \omega') L \delta_{a+b,0} = \begin{pmatrix} \langle \phi_a(\omega) \phi_b(\omega') \rangle & \langle \phi_a(\omega) \psi_b(\omega') \rangle \\ \langle \psi_a(\omega) \psi_b(\omega') \rangle & \langle \psi_a(\omega) \phi_b(\omega') \rangle \end{pmatrix} \quad (\text{B14})$$

with the Kronecker δ -function denoted by $\delta_{a+b,0}$ and the Dirac δ -function by $\delta(\omega) = 2\pi\delta(\omega)$. The propagators are then found to be

$$\left\langle \phi_a(\omega) \tilde{\phi}_b(\omega') \right\rangle_0 = \frac{\Gamma_a(\omega; r) \delta(\omega + \omega') L \delta_{a+b,0}}{\Gamma_a(\omega; r) \Gamma_{-a}(\omega; r) - \gamma^2} \triangleq \overline{\phi_a(\omega) \tilde{\phi}_b(\omega')} \quad (\text{B15a})$$

$$\left\langle \psi_a(\omega) \tilde{\psi}_b(\omega') \right\rangle_0 = \frac{\Gamma_{-a}(\omega; r) \delta(\omega + \omega') L \delta_{a+b,0}}{\Gamma_a(\omega; r) \Gamma_{-a}(\omega; r) - \gamma^2} \triangleq \underbrace{\psi_a(\omega) \tilde{\psi}_b(\omega')}_{\sim\sim\sim\sim\sim} \quad (\text{B15b})$$

$$\left\langle \phi_a(\omega) \tilde{\psi}_b(\omega') \right\rangle_0 = \frac{\gamma \delta(\omega + \omega') L \delta_{a+b,0}}{\Gamma_a(\omega; r) \Gamma_{-a}(\omega; r) - \gamma^2} \triangleq \overline{\phi_a(\omega) \tilde{\psi}_b(\omega')} \quad (\text{B15c})$$

$$\left\langle \psi_a(\omega) \tilde{\phi}_b(\omega') \right\rangle_0 = \frac{\gamma \delta(\omega + \omega') L \delta_{a+b,0}}{\Gamma_a(\omega; r) \Gamma_{-a}(\omega; r) - \gamma^2} \triangleq \underbrace{\psi_a(\omega) \tilde{\phi}_b(\omega')}_{\sim\sim\sim\sim\sim} \quad (\text{B15d})$$

where we have introduced

$$\Gamma_a(\omega; r) = -i\omega + Dk_a^2 - i\omega k_a + r + \gamma \quad (\text{B16})$$

to ease notation.

After Fourier-transforming, the perturbative part of the action, Eq. (B6) reads

$$\mathcal{A}_1 = -\frac{1}{L^3} \sum_{a,b,c} L \delta_{a+b+c,0} \int \ddagger \omega \nu (k_a \tilde{\phi}_a(\omega)) k_b U_b \phi_c(-\omega) + \nu (k_a \tilde{\psi}_a(\omega)) k_b U_b \psi_c(-\omega) \quad (\text{B17})$$

which effectively destroys momentum conservation, as any mismatch $a + c \neq 0$ can be made up by the Fourier modes b of the potential, U_b . Each order in the perturbative expansion thus requires a summation over the momenta, similar to integrating a loop.

The ensuing diagrammatics significantly simplifies the bookkeeping. The external potential vertex may be written as

$$\begin{array}{ccc} \tilde{\phi}_a & \phi_c & \tilde{\psi}_a \quad \psi_b \\ \text{---} & & \text{---} \\ | & & | \\ \text{---} & & \text{---} \\ | & & | \\ \text{---} & & \text{---} \\ \text{---} & & \text{---} \\ \oplus & & \oplus \\ | & & | \\ \text{---} & & \text{---} \\ | & & | \\ \text{---} & & \text{---} \\ \nu U_b & & \nu U_c \end{array} \quad (\text{B18})$$

with the bauble representing the external potential, which supplies the missing momentum. The short, thick dashes across (amputated) propagators indicate diagrammatically the factors k_a and k_b , Eq. (B17). Eq. (B18) corrects the propagators as shown in Eq. (2). Unfortunately, the (Dyson) summation can generally not be performed in closed form, but rather needs to be done order by order in the perturbative parameter ν . How this is done to determine steady-state expectations is described in the next section.

Appendix C: Steady-state density and current

In the following, we present the details of the derivation of the steady-state particle densities

$$\rho_+(x) = \lim_{t_0 \rightarrow -\infty} \langle \phi(x, t) \tilde{\phi}(x_0, t_0) \rangle = \lim_{t_0 \rightarrow -\infty} \langle \phi(x, t) \tilde{\psi}(x_0, t_0) \rangle \quad (\text{C1a})$$

$$\rho_-(x) = \lim_{t_0 \rightarrow -\infty} \langle \psi(x, t) \tilde{\phi}(x_0, t_0) \rangle = \lim_{t_0 \rightarrow -\infty} \langle \psi(x, t) \tilde{\psi}(x_0, t_0) \rangle, \quad (\text{C1b})$$

independent of t and x_0 given the limit to the steady state and ergodicity due to the perturbation theory about vanishing potential at positive tumbling rate γ . We will firstly give a rather general argument about the effect of the limit $t_0 \rightarrow -\infty$ on diagrams, before focusing on the present field theory.

1. General arguments

The diagrammatic expansion of the propagators, Eq. (2) or

$$\langle \phi_a(\omega) \tilde{\phi}_b(\omega') \rangle = \text{---} + \begin{array}{c} \text{---} \\ | \\ \oplus \\ | \\ \text{---} \\ \oplus \\ | \\ \text{---} \end{array} + \begin{array}{c} \text{---} \\ | \\ \oplus \\ | \\ \text{---} \\ | \\ \oplus \\ | \\ \text{---} \end{array} + \dots \quad (\text{C2})$$

$$\langle \psi_a(\omega) \tilde{\psi}_b(\omega') \rangle = \text{~~~~~} + \begin{array}{c} \text{~~~~~} \\ | \\ \oplus \\ | \\ \text{~~~~~} \\ \oplus \\ | \\ \text{~~~~~} \end{array} + \begin{array}{c} \text{~~~~~} \\ | \\ \oplus \\ | \\ \text{~~~~~} \\ | \\ \oplus \\ | \\ \text{~~~~~} \end{array} + \dots \quad (\text{C3})$$

is most easily written in Fourier space, where the steady-state limit $t_0 \rightarrow -\infty$ has the effect of restricting any incoming frequency and momentum to $\omega' = 0$ and $b = 0$. We discuss this mechanism, which is very widely applicable, in the following.

Firstly, any tree-like contribution to, say, $\langle \phi_a(\omega) \tilde{\phi}_b(\omega') \rangle$ has an incoming right bare propagator as well as a number of internal bare propagators, which each “carry” all of ω' . Given the pre-factor of $\delta(\omega + \omega')$ of each diagram, taking the Fourier transform in t and t_0 of such a diagram amounts to identifying the poles p_i in ω' throughout, so that in direct time, the n th order contribution to the propagator generally has the structure

$$\left\langle \phi_a(t) \tilde{\phi}_b(t_0) \mathcal{A}_1^n \right\rangle_0 = \sum_i e^{i(t-t_0)p_i} \mathcal{F}_{ab}(p_i) \quad (\text{C4})$$

with some (complicated) $\mathcal{F}_{ab}(p_i)$ determined by the residues. By causality, all poles in ω' have positive imaginary part, provided the mass r is positive. Taking the limit $t_0 \rightarrow -\infty$ selects those poles that vanish in the limit $r \downarrow 0$. In tree diagrams, these poles are entirely given by the bare propagators, featuring as external or internal legs.

The poles of the bare propagators Eq. (B15) are determined by

$$0 = \Gamma_a(\omega; r) \Gamma_{-a}(\omega; r) - \gamma^2 = \left(i\omega' + Dk_b^2 + r + 2\gamma \right) \left(i\omega' + Dk_b^2 + r \right) + (wk_b)^2 \quad (\text{C5})$$

using $b = -a$ from $\delta_{a+b,0}$ and $\omega' = -\omega$ from $\delta(\omega' + \omega)$ in the numerators of Eqs. (B15). It is immediately clear that any $i\omega' + r$ that solves this equation cannot be arbitrarily small for any $\mathbb{Z} \ni b \neq 0$. This leaves us with requiring $b = 0$, which has one pole that vanishes at $r \downarrow 0$, namely $\omega' = ir$. Taking $t_0 \rightarrow -\infty$ after Fourier transforming and $r \downarrow 0$ therefore leaves only those propagators that have $a = -b = 0$.

Because of the structure of the vertex, Eq. (B17), the perturbative contributions to the full propagators due to tree-level diagrams such as Eq. (2) all have dashed internal and outgoing propagators, *i.e.* they all, except the incoming leg, carry a pre-factor k_a , so that they each vanish for vanishing momentum. Taking therefore the limit $t_0 \rightarrow -\infty$, leaves (of the many residues there might be), only those that do not carry such an extra factor $k_a = 0$ of a momentum. In the present field theory, the only such bare propagator is the incoming leg. We will next determine its value in the limit $t_0 \rightarrow -\infty$ and the effect that this limit has on the rest of the diagram. We can safely assume that this pole is simple, because if it was repeated by being equally the pole of another propagator, its residue must vanish, because any such other propagator is guaranteed to carry a factor of k_a .

At $a = 0$ the poles Eq. (C5) are conveniently written as $(-i\omega + r + 2\gamma)(-i\omega + r) = 0$, leaving a factor of 2γ in the denominator as a residue. As far as the numerators of the propagators are concerned, Eqs. (B15a) and (B15b) produce a factor of $\Gamma_0(-ir; r) \delta(\omega + \omega') L \delta_{a+b,0}$ and Eqs. (B15c) and (B15d) a factor of $\gamma \delta(\omega + \omega') L \delta_{a+b,0}$, which are in fact the same as $\Gamma_0(-ir; r) = \gamma$, Eq. (B16).

This mechanism of taking the Fourier transform in ω' and ω and taking the limit $t_0 \rightarrow -\infty$ after $r \downarrow 0$ thus has the effect of replacing any incoming bare propagator such as $\left\langle \phi_a(t) \tilde{\phi}_b(t_0) \right\rangle_0$ by $\gamma L \delta_{a+b,0} \delta_{b,0} / (2\gamma)$, where $\delta_{b,0}$ enforces that only $b = 0 = -a$ ever contributes. Taking further the inverse Fourier-sum over b , Eq. (B10), and transforming t back to ω then gives

$$\lim_{t_0 \rightarrow -\infty} \lim_{r \downarrow 0} \left\langle \phi_a(\omega) \tilde{\phi}(x_0, t_0) \right\rangle_0 = \frac{1}{L} \sum_b e^{ik_b x_0} \int dt e^{i\omega t} \lim_{t_0 \rightarrow -\infty} \lim_{r \downarrow 0} \left\langle \phi_a(t) \tilde{\phi}_b(t_0) \right\rangle_0 = \frac{1}{2} \delta(\omega) \delta_{a,0} \quad (\text{C6})$$

which is identically the same for all bare propagators Eqs. (B15). Within a diagram the effect of the limit $t_0 \rightarrow -\infty$ is thus a pre-factor determined by the diagram and an amputation, as both ω and a are forced to vanish. Because the internal field $\phi_a(\omega)$ will feature in an integral $\int d\omega$, the $\delta(\omega)$ will simply be integrated out, whereas the sum over the spatial modes, $L^{-1} \sum_a$ will leave behind a factor $1/L$. In summary, the limit $t_0 \rightarrow -\infty$ in a bare propagator is given by Eq. (C6) and in all the diagrams considered here, amounts to an amputation of the incoming leg and a multiplication by of the diagram by $1/(2L)$.

After the removal of the incoming leg and thus setting effectively $-i\omega + r = 0$ throughout a diagram, some residues of the form

$$k_c^2 \left(\Gamma_c(-ir; r) \Gamma_{-c}(-ir; r) - \gamma^2 \right)^{-1} = \frac{k_c^2}{(Dk_c^2)^2 + (w^2 + 2D\gamma)k_c^2} \quad (\text{C7})$$

feature with index c still to be summed over. At $k_c = 0$ such residues are in fact repeated poles of ω' , that are, however, bound to vanish as argued above. Cancelling k_c^2 in numerator and denominator for $c = 0$ nevertheless ignores the fact that the term that gives rise to it,

$$k_c^2 (\Gamma_c(\omega; r)\Gamma_{-c}(\omega; r) - \gamma^2)^{-1} = \frac{k_c^2}{\left(-i\omega + Dk_c^2 + r + 2\gamma\right)\left(-i\omega + Dk_c^2 + r\right) + (wk_c)^2} \quad (\text{C8})$$

strictly vanishes at $c = 0$. This is the reason for the introduction of the indicator function

$$\mathcal{I}_a = 1 - \delta_{a,0} = \begin{cases} 0 & \text{for } a = 0 \\ 1 & \text{otherwise} \end{cases}. \quad (\text{C9})$$

As $c \in \mathbb{Z}$, this is merely a matter of bookkeeping and algebra, not a matter of complex analysis or exchange of limits, as is illustrated by the example

$$\lim_{t_0 \rightarrow -\infty} \lim_{r \downarrow 0} \int \mathrm{d}\omega' e^{-i\omega' t_0} \frac{Dk_c^2}{i\omega' + Dk_c^2 + r} \frac{1}{i\omega' + r} = \begin{cases} 0 & \text{for } c = 0 \\ 1 & \text{otherwise} \end{cases} \quad (\text{C10a})$$

$$\quad (\text{C10b})$$

for any $c \in \mathbb{Z}$.

2. Steady-state density of Run-and-Tumble particles in a periodic potential

On the basis of the mechanism outlined above, we can write down a perturbative expansion Eq. (B9) of the steady-state density, for example

$$\begin{aligned} \lim_{t_0 \rightarrow -\infty} \langle \phi_a(t) \tilde{\phi}(x_0, t_0) \rangle &= \lim_{t_0 \rightarrow -\infty} \langle \phi_a(t) \tilde{\psi}(x_0, t_0) \rangle \\ &= \lim_{t_0 \rightarrow -\infty} \langle \phi_a(t) \tilde{\phi}(x_0, t_0) \rangle_0 + \lim_{t_0 \rightarrow -\infty} \langle \phi_a(t) \tilde{\phi}(x_0, t_0) (-\mathcal{A}_1) \rangle_0 + \dots \end{aligned} \quad (\text{C11})$$

where we have trivially taken the inverse Fourier transform from ω to t . The limit $\lim_{t_0 \rightarrow -\infty} \langle \phi_a(t) \tilde{\phi}(x_0, t_0) \rangle_0 = \delta_{a,0}/2$ is given by Eq. (C6), whereas the higher order terms are most easily calculated using the diagrammatics. The lowest order corrections are of the form

$$\lim_{t_0 \rightarrow -\infty} \langle \phi_a(t) \tilde{\phi}(x_0, t_0) (-\mathcal{A}_1) \rangle_0 \triangleq \begin{array}{c} \text{---} \\ \text{---} \end{array} \begin{array}{c} \text{---} \\ \text{---} \end{array} \quad (\text{C12a})$$

$$\triangleq (-k_a \mathcal{I}_a) \frac{\Gamma_a^0}{\Gamma_a^0 \Gamma_{-a}^0 - \gamma^2} (\nu k_a U_a) \frac{1}{2L} + (-k_a \mathcal{I}_a) \frac{\gamma \mathcal{I}_a}{\Gamma_a^0 \Gamma_{-a}^0 - \gamma^2} (\nu k_a U_a) \frac{1}{2L} \quad (\text{C12b})$$

$$= -\frac{(Dk_a^2 - i\omega k_a + 2\gamma) \mathcal{I}_a \nu U_a}{D^2 k_a^2 + 2D\gamma + \omega^2} \frac{1}{2L} \quad (\text{C12c})$$

where, again, the Fourier transform in ω is easily taken as no ω flows through the diagrams Eq. (C12a), reducing any $\Gamma_a(\omega; r)$ in Eq. (B15) to $\Gamma_a(0; r)$ and further to $\Gamma_a^0 = \Gamma_a(0; 0) = Dk_a^2 - i\omega k_a + \gamma$ as $r \downarrow 0$. To arrive at Eq. (C12b), we have firstly inserted the dash on the outgoing propagator due to the perturbation, $(-k_a \mathcal{I}_a)$, with the indicator function due to the $t_0 \rightarrow -\infty$ mechanism, secondly the propagators Eqs. (B15a) and (B15c) respectively, both evaluated at $\omega = 0$ and $r \downarrow 0$, thirdly the derivative of the potential due to the perturbation and finally a factor $1/(2L)$ due to the $t_0 \rightarrow -\infty$ mechanism. The final line Eq. (C12c) is then a matter of algebra, using $\Gamma_a^0 \Gamma_{-a}^0 - \gamma^2 = k_a^2 (D^2 k_a^2 + 2D\gamma + \omega^2)$.

As all bare propagators will be evaluated at $\omega' = 0$ and $r \downarrow 0$ in the following, we introduce

$X_a = Y_a^*$ and Z_a to ease notation,

$$\left\langle \phi_a(\omega) \tilde{\phi}_b(\omega' = 0) \right\rangle_0 k_{-a} \mathcal{I}_a = \frac{Dk_a^2 - iw k_a + \gamma}{k_a^2 (D^2 k_a^2 + 2D\gamma + w^2)} \delta(\omega) L\delta_{a+b,0} k_{-a} \mathcal{I}_a = X_a \delta(\omega) L\delta_{a+b,0} \quad (\text{C13a})$$

$$\left\langle \psi_a(\omega) \tilde{\psi}_b(\omega' = 0) \right\rangle_0 k_{-a} \mathcal{I}_a = \frac{Dk_a^2 + iw k_a + \gamma}{k_a^2 (D^2 k_a^2 + 2D\gamma + w^2)} \delta(\omega) L\delta_{a+b,0} k_{-a} \mathcal{I}_a = Y_a \delta(\omega) L\delta_{a+b,0} \quad (\text{C13b})$$

$$\left\langle \phi_a(\omega) \tilde{\psi}_b(\omega' = 0) \right\rangle_0 k_{-a} \mathcal{I}_a = \frac{\gamma}{k_a^2 (D^2 k_a^2 + 2D\gamma + w^2)} \delta(\omega) L\delta_{a+b,0} k_{-a} \mathcal{I}_a = Z_a \delta(\omega) L\delta_{a+b,0} \quad (\text{C13c})$$

$$\left\langle \psi_a(\omega) \tilde{\phi}_b(\omega' = 0) \right\rangle_0 k_{-a} \mathcal{I}_a = \frac{\gamma}{k_a^2 (D^2 k_a^2 + 2D\gamma + w^2)} \delta(\omega) L\delta_{a+b,0} k_{-a} \mathcal{I}_a = Z_a \delta(\omega) L\delta_{a+b,0} \quad (\text{C13d})$$

where we have anticipated the factor $k_{-a} \mathcal{I}_a$ that each propagator will pick up.

a. Recurrence relation for density $\rho(x)$ and polarity $\mu(x)$

In the following, we obtain a recurrence relation of the orders in ν of $\rho(x)$ and $\mu(x)$ using their diagrammatic representation. To this end, we introduce a diagrammatic notation for the b th Fourier coefficient of the $(n-1)$ th order steady-state density of right-moving particles

$$\begin{aligned} \nu^{n-1} \rho_{b+}^{(n-1)} &= \lim_{t_0 \rightarrow -\infty} \left\langle \phi_b(t) \tilde{\phi}(x_0, t_0) \frac{(-\mathcal{A}_1)^{n-1}}{(n-1)!} \right\rangle_0 = \lim_{t_0 \rightarrow -\infty} \left\langle \phi_b(t) \tilde{\psi}(x_0, t_0) \frac{(-\mathcal{A}_1)^{n-1}}{(n-1)!} \right\rangle_0 \\ &\triangleq \text{---} \overset{b}{\text{---}} \begin{array}{c} \text{---} \overbrace{\text{---} \underbrace{\text{---}} \text{---}}^{\text{---}} \text{---} \\ \vdots \quad \dots \quad \vdots \\ \circ \quad \dots \quad \circ \end{array} \quad (\text{C14}) \end{aligned}$$

and the $(n-1)$ th order steady-state density of left-moving particles

$$\begin{aligned} \nu^{n-1} \rho_{b-}^{(n-1)} &= \lim_{t_0 \rightarrow -\infty} \left\langle \phi_b(t) \tilde{\phi}(x_0, t_0) \frac{(-\mathcal{A}_1)^{n-1}}{(n-1)!} \right\rangle_0 = \lim_{t_0 \rightarrow -\infty} \left\langle \phi_b(t) \tilde{\psi}(x_0, t_0) \frac{(-\mathcal{A}_1)^{n-1}}{(n-1)!} \right\rangle_0 \\ &\triangleq \begin{array}{c} \text{---} \overbrace{\text{---} \underbrace{\text{---}} \text{---}}^{\text{---}} \text{---} \\ \vdots \quad \dots \quad \vdots \\ \circ \quad \dots \quad \circ \end{array} \quad (\text{C15}) \end{aligned}$$

As indicated by the dots, both diagrams, Eqs. (C14) and (C15), contain $n-1$ potential ‘‘baubles’’ and both are written in terms of ‘‘gluonic’’ propagators $\overbrace{\text{---}}^{\text{---}}$ which we use to represent the sum over all possibilities of connecting the baubles to each other and finally to the external field. Much of what follows is about the bookkeeping of these diagrams. The lowest order is given by Eq. (C6),

$$\rho_{a+}^{(0)} = \rho_{a-}^{(0)} = \frac{1}{2} \delta_{a,0} \ , \quad (\text{C16})$$

after the inverse Fourier transform that simply removes $\delta(\omega)$.

To construct the n order diagrams of both particle species we need to attach a potential bauble to the $n-1$ th order diagrams. Any such potential term Eq. (B17) comes with a summation over all three indices associated with its three terms, namely the potential, a creator field with a derivative and an annihilator field. By adding a further perturbative term in this way, both $\rho_{a+}^{(n)}$ and $\rho_{a-}^{(n)}$ each acquire two contributions due to $\rho_{b+}^{(n-1)}$ and $\rho_{b-}^{(n-1)}$, both connecting to $\rho_{b+}^{(n)}$ and $\rho_{b-}^{(n)}$ using

Eq. (B18) and a suitable propagator Eq. (B15). The resulting terms are

$$\nu^n \rho_{a+}^{(n)} \triangleq \begin{array}{c} a \text{-----} b \\ | \quad | \quad | \quad | \quad | \\ \vdots \quad \vdots \quad \vdots \quad \vdots \quad \vdots \\ \circ \quad \circ \quad \dots \quad \circ \quad \circ \end{array} + \begin{array}{c} a \text{-----} b \\ | \quad | \quad | \quad | \quad | \\ \vdots \quad \vdots \quad \vdots \quad \vdots \quad \vdots \\ \circ \quad \circ \quad \dots \quad \circ \quad \circ \end{array} \quad (\text{C17a})$$

$$\triangleq \frac{1}{L} \sum_b k_{a-b} \nu U_{a-b} \left(X_a \nu^{n-1} \rho_{b+}^{(n-1)} + Z_a \nu^{n-1} \rho_{b-}^{(n-1)} \right) \quad (\text{C17b})$$

and

$$\nu^n \rho_{a-}^{(n)} \triangleq \begin{array}{c} a \text{-----} b \\ | \quad | \quad | \quad | \quad | \\ \vdots \quad \vdots \quad \vdots \quad \vdots \quad \vdots \\ \circ \quad \circ \quad \dots \quad \circ \quad \circ \end{array} + \begin{array}{c} a \text{-----} b \\ | \quad | \quad | \quad | \quad | \\ \vdots \quad \vdots \quad \vdots \quad \vdots \quad \vdots \\ \circ \quad \circ \quad \dots \quad \circ \quad \circ \end{array} \quad (\text{C18a})$$

$$\triangleq \frac{1}{L} \sum_b k_{a-b} \nu U_{a-b} \left(Z_a \nu^{n-1} \rho_{b+}^{(n-1)} + Y_a \nu^{n-1} \rho_{b-}^{(n-1)} \right). \quad (\text{C18b})$$

Using Eqs. (C17) and (C16) with $n = 1$ produces for example Eqs. (C12),

$$\nu \rho_{a+}^{(1)} = \frac{1}{L} k_a \nu U_a (X_a + Z_a) \frac{1}{2} \quad (\text{C19})$$

with Eqs. (C13a) and (C13c).

In the following, it is more instructive to work with the density

$$\rho_a^{(n)} = \rho_{a+}^{(n)} + \rho_{a-}^{(n)} \quad \text{so that} \quad \rho(x) = \frac{1}{L} \sum_{a=-\infty}^{\infty} e^{ik_a x} \sum_{n=0}^{\infty} \nu^n \rho_a^{(n)} \quad (\text{C20a})$$

and the polarity

$$\mu_a^{(n)} = \rho_{a+}^{(n)} - \rho_{a-}^{(n)} \quad \text{so that} \quad \mu(x) = \frac{1}{L} \sum_{a=-\infty}^{\infty} e^{ik_a x} \sum_{n=0}^{\infty} \nu^n \mu_a^{(n)}, \quad (\text{C20b})$$

and write the convolutions Eqs. (C17) and (C18) in terms of a single matrix equation

$$\begin{pmatrix} \rho_a^{(n)} \\ \mu_a^{(n)} \end{pmatrix} = \underline{\underline{M_a}} \sum_{b=-\infty}^{\infty} W_{a-b} \begin{pmatrix} \rho_b^{(n-1)} \\ \mu_b^{(n-1)} \end{pmatrix} \quad (\text{C21})$$

with

$$W_{a-b} = \frac{k_{a-b} U_{a-b}}{L} \quad (\text{C22})$$

and the matrix

$$\underline{\underline{M_a}} = \frac{1}{2} \begin{pmatrix} X_a + Y_a + 2Z_a & X_a - Y_a \\ X_a - Y_a & X_a + Y_a - 2Z_a \end{pmatrix} = \frac{(-k_a) \mathcal{I}_a}{k_a^2 (D^2 k_a^2 + 2D\gamma + w^2)} \begin{pmatrix} Dk_a^2 + 2\gamma & -ik_a \\ -ik_a & Dk_a^2 \end{pmatrix}, \quad (\text{C23})$$

as a function of the mode a , closely related to Eq. (B14). Eqs. (C21) and (C23) are the main result of the present section as they determine density and polarity to arbitrary order in ν . As a sanity check, we may verify that both density $\rho(x)$ and polarity $\mu(x)$, Eqs. (C20), are real, or equivalently that complex conjugates of the modes obey $(\rho_a^{(n)})^* = \rho_{-a}^{(n)}$ and $(\mu_a^{(n)})^* = \mu_{-a}^{(n)}$. This can be done by induction, assuming that $(\rho_a^{(n-1)})^* = \rho_{-a}^{(n-1)}$ and $(\mu_a^{(n-1)})^* = \mu_{-a}^{(n-1)}$, and further observing that $(\underline{\underline{M_a}})^* = -\underline{\underline{M_{-a}}}$ from Eq. (C23) and that a real external potential implies

$(W_{a-b})^* = -W_{b-a}$. From Eq. (C16) we have

$$\begin{pmatrix} \rho_a^{(0)} \\ \mu_a^{(0)} \end{pmatrix} = \begin{pmatrix} 1 \\ 0 \end{pmatrix} \delta_{a,0} \quad (\text{C24})$$

as induction basis and, more importantly, as the starting point for the systematic calculation Eq. (C21) of the modes of the density and polarity Eq. (C20). With that established, we may write Eq. (6)

$$\begin{pmatrix} \rho_{a_1}^{(n)} \\ \mu_{a_1}^{(n)} \end{pmatrix} = \underline{\underline{M_{a_1}}} \sum_{a_2, a_3, \dots, a_n = -\infty}^{\infty} W_{a_1 - a_2} \underline{\underline{M_{a_2}}} W_{a_2 - a_3} \underline{\underline{M_{a_3}}} \cdots W_{a_{n-1} - a_n} \underline{\underline{M_{a_n}}} W_{a_n} \begin{pmatrix} 1 \\ 0 \end{pmatrix}, \quad (\text{C25})$$

with each of the $n - 1$ indices running from $-\infty$ to ∞ . We will now turn our attention to the steady-state current.

3. Steady-state current

From Fick's law of diffusion and the coupled Fokker-Planck equation, the steady-state probability current $J(x)$ reads

$$J(x) = w\mu(x) - \nu\rho(x)U'(x) - D\partial_x\rho(x), \quad (\text{C26})$$

which in the steady state must in fact be constant in x . We will demonstrate this property perturbatively, order by order in ν . To this end, we introduce the inverse Fourier-transforms

$$\rho^{(n)}(x) = \frac{1}{L} \sum_{a=-\infty}^{\infty} e^{ik_a x} \rho_a^{(n)} \quad (\text{C27a})$$

$$\mu^{(n)}(x) = \frac{1}{L} \sum_{a=-\infty}^{\infty} e^{ik_a x} \mu_a^{(n)} \quad (\text{C27b})$$

of the n th order Fourier coefficients $\rho_a^{(n)}$ and $\mu_a^{(n)}$, similar to Eq. (C20). The steady-state current $J(x)$ in Eq. (C26) may then be written order by order in ν ,

$$J(x) = \sum_{n=0}^{\infty} \nu^n J^{(n)}(x) \quad (\text{C28})$$

with $J^{(n)}(x)$ for $n > 0$ extracted from Eq. (C26) by identifying terms of order n in ν ,

$$J^{(n)}(x) = w\mu^{(n)}(x) - \rho^{(n-1)}(x)U'(x) - D\partial_x\rho^{(n)}(x). \quad (\text{C29})$$

We will proceed by showing that $J^{(n)}(x)$ is constant in x and can easily be expressed in terms of the Fourier coefficients $\rho_a^{(n)}$ and $\mu_a^{(n)}$ using Eqs. (C27) and (C21),

$$J^{(n)}(x) = -\rho^{(n-1)}(x)U'(x) \frac{1}{L} \sum_{a,b=-\infty}^{\infty} e^{ik_a x} \begin{pmatrix} -Dik_a \\ w \end{pmatrix}^{\top} \underline{\underline{M_a}} W_{a-b} \begin{pmatrix} \rho_b^{(n-1)} \\ \mu_b^{(n-1)} \end{pmatrix}. \quad (\text{C30})$$

By direct calculation the linear algebra involving $\underline{\underline{M_a}}$, Eq. (C23), simplifies drastically,

$$\begin{pmatrix} -Dik_a \\ w \end{pmatrix}^{\top} \underline{\underline{M_a}} = i\mathcal{I}_a \begin{pmatrix} 1 \\ 0 \end{pmatrix}^{\top}. \quad (\text{C31})$$

The first term in Eq. (C30) can be written in modes as

$$\rho^{(n-1)}(x)U'(x) = \frac{1}{L^2} \sum_{a,b=-\infty}^{\infty} e^{ik_a x} e^{ik_b x} \rho_b^{(n-1)} ik_a U_a = \frac{i}{L} \sum_{a,b=-\infty}^{\infty} e^{ik_a x} \rho_b^{(n-1)} W_{a-b} \quad (\text{C32})$$

with Eqs. (B11) and (C22) and using $k_{a-b} + k_b = k_a$ after shifting the dummy index a by $-b$, so that the final expression is the inverse Fourier-transform of a convolution. Using Eqs. (C31) and (C32) in Eq. (C30) finally gives

$$J^{(n)}(x) = \frac{i}{L} \sum_{a,b=-\infty}^{\infty} e^{ik_a x} \rho_b^{(n-1)} W_{a-b} (-1 + \mathcal{I}_a) = -\frac{i}{L} \sum_{b=-\infty}^{\infty} \rho_b^{(n-1)} W_{-b} \quad (\text{C33})$$

using the definition of the indicator function, $\mathcal{I}_a = 1 - \delta_{a,0}$. Eq. (C33) not only shows that every perturbative order of the steady-state current is independent of the position x , as it should be, but also expresses the current to order n in terms of the density to order $n - 1$. The 0th order of current follows immediately from Eq. (C26) as

$$J^{(0)}(x) = w\mu^{(0)}(x) - D\partial_x \rho^{(0)}(x) = 0 \quad (\text{C34})$$

because $\mu^{(0)}(x) = 0$ and $\rho^{(0)}(x) = 1/L$ from the inverse Fourier transform of Eq. (C24).

Eq. (C33) is the main result of the present section. With Eq. (C25) we can write it as Eq. (7),

$$J^{(n)}(x) = -\frac{i}{L} \sum_{a_1, a_2, \dots, a_{n-1} = -\infty}^{\infty} W_{-a_1} W_{a_1 - a_2} \cdots W_{a_{n-2} - a_{n-1}} W_{a_{n-1}} \begin{pmatrix} 1 \\ 0 \end{pmatrix}^\top \underline{\underline{M_{a_1}}} \underline{\underline{M_{a_2}}} \cdots \underline{\underline{M_{a_{n-1}}}} \begin{pmatrix} 1 \\ 0 \end{pmatrix} \quad (\text{C35})$$

which contains n factors of W and $n - 1$ factors of the matrix $\underline{\underline{M_a}}$. It will prove useful to relabel the $n - 1$ dummy variables a_i by n dummy variables $b_1 = -a_1$, $b_2 = a_1 - a_2$, $b_3 = a_2 - a_3$, \dots , $b_{n-1} = a_{n-2} - a_{n-1}$, $b_n = a_{n-1}$, imposing that $\sum_{i=1}^n b_i = 0$ by a Kronecker δ -function,

$$J^{(n)}(x) = -\frac{i}{L} \sum_{b_1, b_2, \dots, b_n = -\infty}^{\infty} \delta_{b_1 + b_2 + \dots + b_n, 0} W_{b_1} W_{b_2} \cdots W_{b_{n-1}} W_{b_n} \times \begin{pmatrix} 1 \\ 0 \end{pmatrix}^\top \underline{\underline{M_{-b_1}}} \underline{\underline{M_{-(b_1+b_2)}}} \underline{\underline{M_{-(b_1+b_2+b_3)}}} \cdots \underline{\underline{M_{-(b_1+b_2+\dots+b_{n-1})}}} \begin{pmatrix} 1 \\ 0 \end{pmatrix}. \quad (\text{C36})$$

In Suppl. E we consider properties of the steady-state current generally and in relation to the potential.

Appendix D: Comparison between the field theory and the exact result [4] for a piece-wise linear potential

In this section, we compare our field-theoretic result of the steady-state current J to the exact result [4]. We consider an RnT particle in a periodic, piece-wise linear ratchet potential $U(x) = U(x + L)$ of the form

$$U(x) = \begin{cases} U_0 \frac{x}{\alpha L} & \text{for } x \in [0, \alpha L) \\ U_0 \frac{L-x}{(1-\alpha)L} & \text{for } x \in [\alpha L, L) \end{cases} \quad (\text{D1})$$

as shown in Fig. D1.

The Fokker-Planck equations for RnT particles in a piece-wise linear potential are most easily written down by distinguishing the two intervals $x \in [0, \alpha L)$, by, say, superscript $[i] = [1]$ and

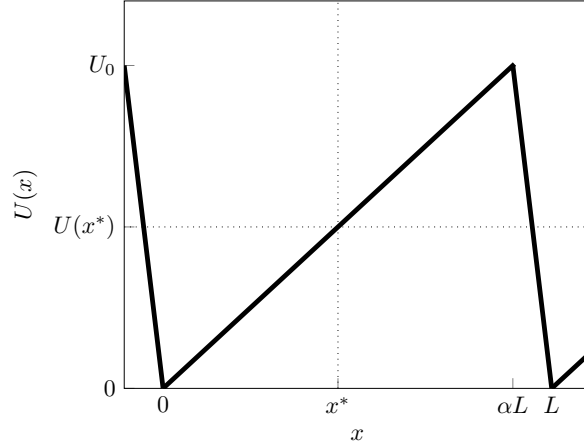


FIG. D1: The periodic, piece-wise linear ratchet described by Eq. (D1) with $\alpha = 0.9$. The ratchet has $U(0) = 0$ rises up to $U(\alpha L) = U_0$ and descends again to $U(L) = 0$. The point $x^* = \alpha L/2$ marks the point where $U(x^* + x) - U(x^*) = U(x^*) - U(x^* - x)$ with $U(x^*) = U_0/2$, Eq. (E1), Suppl. E.

$x \in [\alpha L, L)$ by, say, superscript $[i] = [2]$, so that

$$\begin{aligned} \partial_t \rho_+^{[i]}(x, t) &= -\partial_x[(w - \nu U'^{[i]})\rho_+^{[i]}(x, t)] - \gamma(\rho_+^{[i]}(x, t) - \rho_-^{[i]}(x, t)) + D\partial_x^2 \rho_+^{[i]}(x, t) \\ \partial_t \rho_-^{[i]}(x, t) &= -\partial_x[(-w - \nu U'^{[i]})\rho_-^{[i]}(x, t)] - \gamma(\rho_-^{[i]}(x, t) - \rho_+^{[i]}(x, t)) + D\partial_x^2 \rho_-^{[i]}(x, t) \end{aligned} \quad (\text{D2a})$$

with constant slopes $U'^{[1]} = U_0/(\alpha L)$ and $U'^{[2]} = -U_0/((1 - \alpha)L)$. Similar to the main text, the densities $\rho_+^{[i]}(x, t)$ and $\rho_-^{[i]}(x, t)$ refer to the right-moving and the left-moving particles respectively. Solving this system of equations is greatly facilitated by the slopes being piece-wise constant.

Following the procedure outlined in [4], the steady-state densities $\rho_{\pm}^{[i]}(x)$ are determined by making the ansatz $\rho_{\pm}^{[i]} = Z_{\pm}^{[i]} e^{\lambda^{[i]} x}$, to find 4 linearly independent solutions of Eqs. (D2) for $i = 1, 2$ and both particle species ρ_{\pm} , and solving two coupled quadratic characteristic equations for the eigenvalues. One of those always vanishes, while the others can be relabelled as $\alpha^{[i]}$, $\beta^{[i]}$ and $\gamma^{[i]}$, producing the ansatz

$$\rho_{\pm}^{[i]}(x) = A_{\pm}^{[i]} e^{\alpha^{[i]} x} + B_{\pm}^{[i]} e^{\beta^{[i]} x} + C_{\pm}^{[i]} e^{\gamma^{[i]} x} + D_{\pm}, \quad (\text{D3})$$

which leaves 16 amplitudes to be determined: $A_+^{[1]}$, $A_-^{[1]}$, $A_+^{[2]}$, \dots , $D_-^{[2]}$.

The 16 amplitudes are determined by substituting Eqs. (D3) into Eqs. (D2) at steady state, when the left hand side of the latter vanishes. As a result, the pre-factor of every linearly independent exponential on the right has to vanish, fixing the ratios $A_+^{[i]}/A_-^{[i]}$, $B_+^{[i]}/B_-^{[i]}$, $C_+^{[i]}/C_-^{[i]}$ and $D_+^{[i]}/D_-^{[i]}$ in terms of system parameters for both $i = 1, 2$, which amounts to 8 equations for 16 unknowns. A further 8 equations are obtained by matching conditions at the boundaries of intervals $i = 1$ and $i = 2$, more specifically for the density, $\rho_{\pm}^{[1]}(0) = \rho_{\pm}^{[2]}(L)$ and $\rho_{\pm}^{[1]}(\alpha L) = \rho_{\pm}^{[2]}(\alpha L)$, and correspondingly for the current $J_{\pm}^{[i]}(x) = (\pm w - \nu U'^{[i]} - d/dx)\rho_{\pm}^{[i]}(x)$. It turns out that only 15 of those 16 equations are linearly independent, as expected in a homogeneous, linear system of equations. The final equation is in fact obtained by demanding in addition overall normalisation of the density. This procedure, best done in a computational algebra system [49], results in the density and the current being determined in closed form.

To compare to our field-theory, we choose the height of the piece-wise linear potential $U(x)$ in Eq. (D1) by setting $U_0 = 1$ and vary the coupling ν in Eqs. (D2). Density and current are then determined through the procedure outlined above.

The field-theoretic approach on the other hand is based on the Fourier coefficients of the potential Eq. (D1). Taking the first 200 such modes,

$$U_a = \frac{U_0 (1 - e^{-2i\pi a \alpha})}{4\pi^2 a^2 \alpha (\alpha - 1)}, \quad (\text{D4})$$

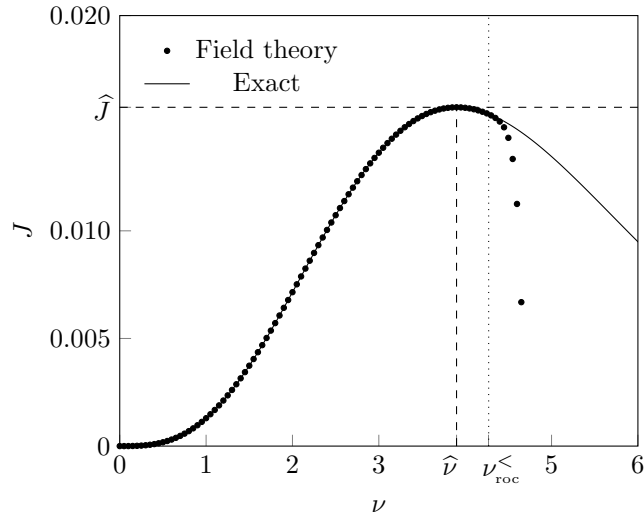


FIG. D2: Comparison of the present field-theoretic result (filled circles) for the steady-state current and the exact solution [4] (solid line) for a piece-wise linear ratchet potential Eq. (D1) with $\alpha = 0.9$ and $U_0 = 1$ as shown in Fig. D1. The other parameters are $w = 1, \gamma = 5, D = 1$ and $L = 1$. The field theoretic results are based on 200 Fourier coefficients and up to 75 orders in ν . The agreement is perfect (deviation of less than 0.15% up until $\nu_{\text{roc}}^< = 4.272 \dots$ the radius of convergence estimated via Eq. (9) and shown as a dotted vertical line. Beyond that, the current due to the field theory diverges sharply. The coupling ν that produces the best current $\hat{J} = 0.015739 \dots$ in this potential is $\hat{\nu} = 3.90 \dots$, where even the shallow part of the potential has a slope greater than the self-propulsion speed, $\hat{\nu}U_0/(\alpha L) = 3.9 \cdot 1/(0.9 \cdot 1) > w = 1$, indicating that transport is dominated by diffusion.

for $a = -200, -199, \dots, 200$, we have calculated the steady-state current J to order 75 in ν . A comparison between this field-theoretic result and the exact result obtained above is shown in Fig. D2. It shows perfect agreement for ν up to the radius of convergence $\nu_{\text{roc}}^< = 4.272 \dots$ estimated via Eq. (9).

Appendix E: Symmetry properties of the steady-state current

In the following we derive some general properties of the steady-state current on the basis of Eqs. (C33) and (C21), that hold to all orders of the perturbation theory. We may briefly consider an odd potential, $U(-x) = -U(x)$, or, given periodicity, more generally a potential with

$$U(x^* + x) - U(x^*) = U(x^*) - U(x^* - x) \quad (\text{E1})$$

allowing for some offset $U(x^*)$ and a more general point of inversion x^* . An example is shown in Fig. D1. If such a potential Eq. (E1) sustains a finite current, it must revert if the coupling changes sign, $\nu \mapsto -\nu$ because by Eq. (E1) this is equivalent to mirroring space $x^* + x \mapsto x^* - x$. We conclude that the expansion of the steady-state current Eq. (C28) of RnT particles *in such a potential* Eq. (E1) must be odd in ν , in other words, $J^{(2n)} = 0$ for $n \in \mathbb{N}$.

It is far from obvious why this should be the case for a general potential. In [34] an argument is sketched that time reversal $z(t) = x(T - t)$ of trajectories $x(t)$ obeying, say,

$$\dot{x} = -\nu U'(x) + \xi_x(t) \quad (\text{E2})$$

with white noise ξ_x are generally solutions of the Langevin equation

$$\dot{z} = \nu U'(z) + \xi_z(t) \quad (\text{E3})$$

with white noise ξ_z distributed identically to ξ_x . The time reversal from Eq. (E2) to (E3) apparently amounts to a change of sign of the coupling ν to $-\nu$ and clearly inverts the total displacement $z(T) - z(0) = -(x(T) - x(0))$. However, in order to conclude that time reversal reverts the *steady-state* current, one has to show that the probabilistic weight of trajectories is unchanged under time

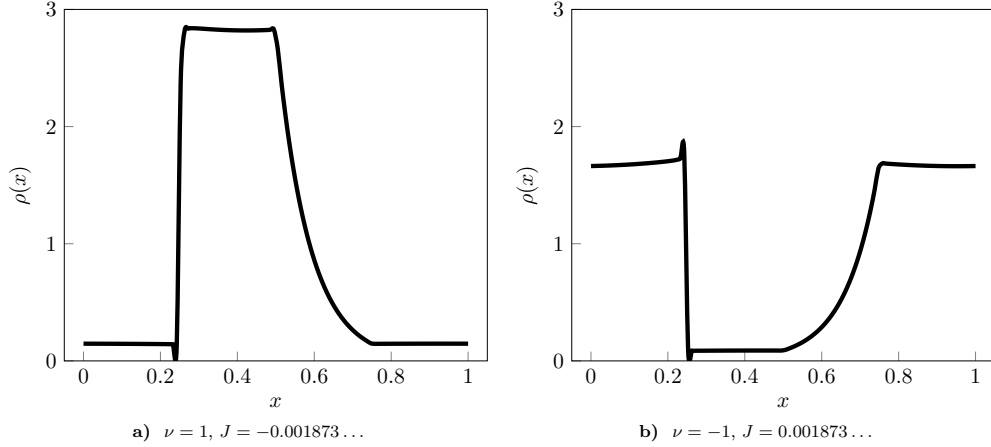


FIG. E1: Particle density $\rho(x)$ for an RnT particle in the periodic “hurdle” potential $U(x)$ Eq. (E4) shown in Fig. E2, based on 100 modes calculated perturbatively to 75th order in ν . Even when the density profiles cannot be related by a simple geometrical transformation, the steady-state currents are simple the negative of each other. Parameters: $D = 1$, $w = 1$, $L = 1$ and $\gamma = 1$, so that $Pe = Qe = \kappa = 1$.

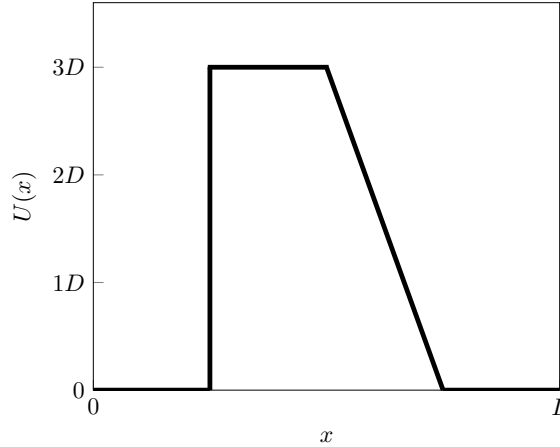


FIG. E2: The “hurdle” potential Eq. (E4), whose resulting RnT particle density is shown in Fig. E1a.

reversal. To put it more succinctly, one has to show that typical steady-state trajectories $x(t)$ of Eq. (E2) are typical steady-state trajectories $z(t)$ of Eq. (E3). That this is generally not the case can be seen in the counter example of a harmonic $U(x) = x^2/2$, where only one of the two Eqs. (E2) and (E3) has a stationary state at all. We conclude that there is no such simple argument as to why the steady-state current is generally odd in ν .

To illustrate the subtleties further, we show in Fig. E1a the particle density $\rho(x)$ of RnT particles in the “hurdle” potential $U(x)$

$$U(x) = \begin{cases} 0 & x \in [0, \frac{L}{4}) \\ 3D & x \in [\frac{L}{4}, \frac{L}{2}) \\ (-12\frac{x}{L} + 9)D & x \in [\frac{L}{2}, \frac{3L}{4}) \\ 0 & x \in [\frac{3L}{4}, L) \end{cases} \quad (\text{E4})$$

shown in Fig. E2 for $\nu = 1$. This is contrasted by Fig. E1b, which shows the particle density for the inverted potential, *i.e.* for the potential Fig. E2 but with coupling $\nu = -1$. The two density profiles are clearly and obviously very distinct, even when they both seem to suffer slightly from the Gibbs phenomenon. While they share some features, there is also no simple geometrical transformation that maps one density profile to the other, and surely not one that is its own inverse as is $\nu \mapsto -\nu$.

For example, both densities being convex from below for the sloped region $x \in [L/2, 3L/4)$ makes it impossible to, say, mirror and overlay the two. The steady-state trajectories in the potential $U(x)$ of Eq. (E4) produce therefore demonstrably a very different density $\rho(x)$ compared to $-U(x)$. And yet, we find that the steady-state currents in the two setups are indeed simply the negative of each other. The following section derives this property perturbatively.

1. The steady-state current J is odd in ν

In the present section we show that changing the sign of ν of the potential simply reverses the steady-state current of RnT particles, despite the density $\rho(x)$ showing none such simple relationship as outlined above. We will do so by showing $J^{(n)} = (-1)^n J^{(n)}$, *i.e.* $J^{(n)} = 0$ for all even n .

The starting point for the derivation is Eq. (C36), where we will rearrange the products of $\underline{\underline{M}}_b$ to arrive at the desired expression. The key observation is that the complex matrix $\underline{\underline{M}}_b$, Eq. (C23), is symmetric (rather than Hermitian), with purely real entries along the diagonal and purely imaginary off-diagonal elements. Firstly, the symmetry implies

$$\mathbf{d}^\top \underline{\underline{M}}_{c_1} \underline{\underline{M}}_{c_2} \cdots \underline{\underline{M}}_{c_{n-1}} \mathbf{e} = \mathbf{e}^\top \underline{\underline{M}}_{c_{n-1}} \underline{\underline{M}}_{c_{n-2}} \cdots \underline{\underline{M}}_{c_1} \mathbf{d}, \quad (\text{E5})$$

for arbitrary vectors \mathbf{e} and \mathbf{d} , so that Eq. (C36), that has $\mathbf{e} = \mathbf{d} = (1, 0)^\top$, is invariant under the inversion of the sequence of Fourier-indices in the product of $\underline{\underline{M}}_b$.

Secondly, the make-up of the elements of $\underline{\underline{M}}_b$, namely purely real diagonal elements and purely imaginary off-diagonal elements, means that any product of $\underline{\underline{M}}_b$ has the same property, so that

$$\begin{pmatrix} 1 \\ 0 \end{pmatrix}^\top \underline{\underline{M}}_{c_1} \underline{\underline{M}}_{c_2} \cdots \underline{\underline{M}}_{c_{n-1}} \begin{pmatrix} 1 \\ 0 \end{pmatrix} \in \mathbb{R}. \quad (\text{E6})$$

Taking the complex conjugate of this expression thus leaves it unchanged. By the definition Eq. (C23), the complex conjugate can be written as $(\underline{\underline{M}}_a)^* = -\underline{\underline{M}}_{-a}$, so that

$$\begin{pmatrix} 1 \\ 0 \end{pmatrix}^\top \underline{\underline{M}}_{c_1} \underline{\underline{M}}_{c_2} \cdots \underline{\underline{M}}_{c_{n-1}} \begin{pmatrix} 1 \\ 0 \end{pmatrix} = (-1)^{n-1} \begin{pmatrix} 1 \\ 0 \end{pmatrix}^\top \underline{\underline{M}}_{-c_1} \underline{\underline{M}}_{-c_2} \cdots \underline{\underline{M}}_{-c_{n-1}} \begin{pmatrix} 1 \\ 0 \end{pmatrix}. \quad (\text{E7})$$

Applying then Eq. (E5) followed by Eq. (E7) to Eq. (C36) gives

$$\begin{aligned} J^{(n)}(x) &= -(-1)^{n-1} \frac{\hat{i}}{L} \sum_{b_1, b_2, \dots, b_n = -\infty} \delta_{b_1 + b_2 + \dots + b_n, 0} W_{b_1} W_{b_2} \cdots W_{b_{n-1}} W_{b_n} \\ &\quad \times \begin{pmatrix} 1 \\ 0 \end{pmatrix}^\top \underline{\underline{M}}_{b_1 + b_2 + \dots + b_{n-1}} \underline{\underline{M}}_{b_1 + b_2 + \dots + b_{n-2}} \cdots \underline{\underline{M}}_{b_1 + b_2} \underline{\underline{M}}_{b_1} \begin{pmatrix} 1 \\ 0 \end{pmatrix}. \end{aligned} \quad (\text{E8})$$

Because $\sum_{i=1}^n b_i = 0$, each of the matrices on the right hand side of Eq. (E8) may be indexed alternatively by $b_1 + b_2 + \dots + b_{n-1} = -b_n$, $b_1 + b_2 + \dots + b_{n-2} = -(b_n + b_{n-1})$, \dots , $b_1 + b_2 = -(b_n + b_{n-1} + \dots + b_3)$ and $b_1 = -(b_n + b_{n-1} + \dots + b_2)$, resulting in

$$\begin{aligned} J^{(n)}(x) &= -(-1)^{n-1} \frac{\hat{i}}{L} \sum_{b_1, b_2, \dots, b_n = -\infty} \delta_{b_1 + b_2 + \dots + b_n, 0} W_{b_1} W_{b_2} \cdots W_{b_{n-1}} W_{b_n} \\ &\quad \times \begin{pmatrix} 1 \\ 0 \end{pmatrix}^\top \underline{\underline{M}}_{-b_n} \underline{\underline{M}}_{-(b_n + b_{n-1})} \cdots \underline{\underline{M}}_{-(b_n + b_{n-1} + \dots + b_3)} \underline{\underline{M}}_{-(b_n + b_{n-1} + \dots + b_2)} \begin{pmatrix} 1 \\ 0 \end{pmatrix}, \end{aligned} \quad (\text{E9})$$

before “mirroring” the indices’ indices, $c_i = b_{n+1-i}$, so that

$$J^{(n)}(x) = -(-1)^{n-1} \frac{i}{L} \sum_{c_1, c_2, \dots, c_n = -\infty} \delta_{c_1+c_2+\dots+c_n, 0} W_{c_n} W_{c_{n-1}} \cdots W_{c_2} W_{c_1} \\ \times \begin{pmatrix} 1 \\ 0 \end{pmatrix}^\top \underline{\underline{M_{-c_1}}} \underline{\underline{M_{-(c_1+c_2)}}} \cdots \underline{\underline{M_{-(c_1+b_2+\dots+c_{n-2})}}} \underline{\underline{M_{-(c_1+b_2+\dots+c_{n-1})}}} \begin{pmatrix} 1 \\ 0 \end{pmatrix}. \quad (\text{E10})$$

As the factors W_{c_i} are scalars, Eq. (E10) is identical to Eq. (C36) up to a factor of $(-1)^{n-1}$, which produces the desired identity

$$J^{(n)}(x) = (-1)^{n-1} J^{(n)}(x), \quad (\text{E11})$$

which implies that $J^{(n)}(x)$ vanishes for even n . This is the main result of the present section. It follows immediately, that J , Eq. (8), is odd in ν and thus changes sign when ν does.

2. The steady-state current vanishes in potentials with only odd Fourier coefficients

We first show that potentials whose even Fourier coefficients all vanish obey

$$U(x) = -U(x + L/2) \quad (\text{E12})$$

and vice versa and are thus identical to those that have been dubbed “supersymmetric” [34].

Firstly, if $U_a = 0$ for all even a , then Eq. (B11) gives

$$U(x + L/2) = \frac{1}{L} \sum_{a=-\infty}^{\infty} e^{ik_a(x+L/2)} U_a = -U(x) \quad (\text{E13})$$

using that $\exp(ik_a(x + L/2)) = (-1)^a \exp(ik_a x)$ and only odd a enters.

Secondly, if $U(x) = U(x + L/2)$, then Eq. (B11) gives

$$U_a = - \int_0^L dx e^{-ik_a x} U(x + L/2) = -(-1)^a \int_{L/2}^{3L/2} dx e^{-ik_a x} U(x) = -(-1)^a U_a, \quad (\text{E14})$$

which means that U_a must vanish for even a .

In the following we demonstrate that the steady-state current vanishes if $U_a = 0$ for all even a .

The potential enters into the perturbative expansion Eq. (C36) of the steady-state current only via W_a Eq. (C22). It features in Eq. (C36) as a product involving all n indices b_1, b_2, \dots, b_n . If W_a vanishes for all even a , then all indices b_1, b_2, \dots, b_n need to be odd in order for the product $W_{b_1} W_{b_2} \dots W_{b_n}$ to be non-zero. However, if all indices b_i are odd, then the sum of an odd number of them cannot possibly vanish, $\sum_{i=1}^n b_i \neq 0$, so that $\delta_{b_1+b_2+\dots+b_n} = 0$ for odd n . It follows that $J^{(n)}$ vanishes for all odd n if U_a vanishes for all even a .

In Suppl. E1 we have demonstrated that $J^{(n)}$ vanishes generally for even n . If $J^{(n)}$ also vanishes for all odd n , then it must vanish overall. In summary, if U_a vanishes for all even a , which is equivalent to saying that the potential is supersymmetric, then J vanishes.

3. The steady-state current vanishes in potentials even about some x^*

The steady-state current of RnT particles in a potential even about x^* ,

$$U(x^* + x) = U(x^* - x) \quad (\text{E15})$$

vanishes trivially because there is no preferred direction. In the following, we rederive this property perturbatively from the expression for the current Eq. (C36).

From Eq. (E15), we derive for the Fourier coefficients using Eq. (B11),

$$\begin{aligned} e^{ik_a x^*} U_a &= e^{ik_a x^*} \int_0^L dx e^{-ik_a(x+x^*)} U(x^* + x) = \int_0^L dx e^{-ik_a x} U(x^* - x) \\ &= e^{-ik_a x^*} \int_0^L dx e^{ik_a(x^*-x)} U(x^* - x) = e^{-ik_a x^*} U_{-a} . \end{aligned} \quad (\text{E16})$$

Considering now the product of W_b , Eq. (C22), in Eq. (C36), it generally has the property

$$\begin{aligned} (W_{b_1} W_{b_2} \cdots W_{b_n}) + (W_{-b_1} W_{-b_2} \cdots W_{-b_n}) \\ = L^{-n} k_{b_1} k_{b_2} \cdots k_{b_n} \left(U_{b_1} U_{b_2} \cdots U_{b_n} + (-1)^n U_{-b_1} U_{-b_2} \cdots U_{-b_n} \right) , \end{aligned} \quad (\text{E17})$$

With Eq. (E16), the product of modes of the potential obeys

$$U_{b_1} U_{b_2} \cdots U_{b_n} = e^{-2i \sum_{a=1}^n k_a x^*} U_{-b_1} U_{-b_2} \cdots U_{-b_n} = U_{-b_1} U_{-b_2} \cdots U_{-b_n} , \quad (\text{E18})$$

provided $\sum_{i=1}^n k_{b_i} = (2\pi/L) \sum_{i=1}^n b_i = 0$, as is enforced by the Kronecker δ -function in Eq. (C36). For a potential even about some x^* , we thus have

$$\begin{aligned} \delta_{b_1+b_2+\dots+b_n,0} (W_{b_1} W_{b_2} \cdots W_{b_n} + W_{-b_1} W_{-b_2} \cdots W_{-b_n}) \\ = \delta_{b_1+b_2+\dots+b_n,0} L^{-n} k_{b_1} k_{b_2} \cdots k_{b_n} \times \begin{cases} 2U_{b_1} U_{b_2} \cdots U_{b_n} & \text{for } n \text{ even} \\ 0 & \text{for } n \text{ odd} . \end{cases} \end{aligned} \quad (\text{E19})$$

This identity can be used in the expression for the steady-state current Eq. (C36) once it has been suitably rewritten. To this end, we double up all terms in Eq. (C36),

$$\begin{aligned} 2J^{(n)}(x) &= -\frac{i}{L} \sum_{b_1, b_2, \dots, b_n = -\infty}^{\infty} \delta_{b_1+b_2+\dots+b_n,0} \\ &\times \left\{ W_{b_1} W_{b_2} \cdots W_{b_{n-1}} W_{b_n} \begin{pmatrix} 1 \\ 0 \end{pmatrix}^T \underline{\underline{M_{-b_1}}} \underline{\underline{M_{-(b_1+b_2)}}} \cdots \underline{\underline{M_{-(b_1+b_2+\dots+b_{n-1})}}} \begin{pmatrix} 1 \\ 0 \end{pmatrix} \right. \\ &\left. + W_{-b_1} W_{-b_2} \cdots W_{-b_{n-1}} W_{-b_n} (-1)^{n-1} \begin{pmatrix} 1 \\ 0 \end{pmatrix}^T \underline{\underline{M_{b_1}}} \underline{\underline{M_{b_1+b_2}}} \cdots \underline{\underline{M_{b_1+b_2+\dots+b_{n-1}}}} \begin{pmatrix} 1 \\ 0 \end{pmatrix} \right\} , \end{aligned} \quad (\text{E20})$$

which by means of Eq. (E7) simplifies to

$$\begin{aligned} 2J^{(n)}(x) &= -\frac{i}{L} \sum_{b_1, b_2, \dots, b_n = -\infty}^{\infty} \delta_{b_1+b_2+\dots+b_n,0} \begin{pmatrix} 1 \\ 0 \end{pmatrix}^T \underline{\underline{M_{-b_1}}} \underline{\underline{M_{-(b_1+b_2)}}} \cdots \underline{\underline{M_{-(b_1+b_2+\dots+b_{n-1})}}} \begin{pmatrix} 1 \\ 0 \end{pmatrix} \\ &\times \left\{ W_{b_1} W_{b_2} \cdots W_{b_{n-1}} W_{b_n} + (-1)^{n-1} W_{-b_1} W_{-b_2} \cdots W_{-b_{n-1}} W_{-b_n} \right\} . \end{aligned} \quad (\text{E21})$$

If the potential is even, then Eq. (E19) can be used on the right hand side for odd n , where $(-1)^{n-1} = 1$, so that

$$2J^{(n)}(x) = 0 \quad \text{for odd } n \text{ if the potential is even, Eq. (E15)} . \quad (\text{E22})$$

As $J^{(n)}(x) = 0$ for all even n , it implies that the steady-state current vanishes altogether. In other words, even potentials, Eq. (E15), have no steady-state current, $J(x) = 0$.